Materials Today Bio 26 (2024) 101064

Contents lists available at ScienceDirect

Materials Today Bio

journal homepage: www.journals.elsevier.com/materials-today-bio

Conductive and alignment-optimized porous fiber conduits with electrical stimulation for peripheral nerve regeneration

Kai Liu [a,b], Shuai Yan [d], Yao Liu [b,e], Jianfeng Liu [a,b], Ruijun Li [a,b], Lirong Zhao [c,**], Bin Liu [a,b,*]

[a] Department of Hand and Foot Surgery, Orthopedics Center, The First Hospital of Jilin University, Changchun, 130021, China
[b] Engineering Laboratory of Tissue Engineering Biomaterials of Jilin Province, Changchun, 130021, China
[c] Department of Ultrasound, The First Hospital of Jilin University, Changchun, 130021, China
[d] Department of Operating Room, The First Hospital of Jilin University, Changchun, 130021, China
[e] Department of Sport Medicine, Orthopedics Center, First Hospital of Jilin University, Changchun, 130021, China

ARTICLE INFO

Keywords:
Peripheral nerve defect
Nerve guide conduit
Electrospinning fibers
Conductive coating
Electrical stimulation

ABSTRACT

Autologous nerve transplantation (ANT) is currently considered the gold standard for treating long-distance peripheral nerve defects. However, several challenges associated with ANT, such as limited availability of donors, donor site injury, mismatched nerve diameters, and local neuroma formation, remain unresolved. To address these issues comprehensively, we have developed porous poly(lactic-*co*-glycolic acid) (PLGA) electrospinning fiber nerve guide conduits (NGCs) that are optimized in terms of alignment and conductive coating to facilitate peripheral nerve regeneration (PNR) under electrical stimulation (ES). The physicochemical and biological properties of aligned porous PLGA fibers and poly(3,4-ethylenedioxythiophene):polystyrene sodium sulfonate (PEDOT:PSS) coatings were characterized through assessments of electrical conductivity, surface morphology, mechanical properties, hydrophilicity, and cell proliferation. Material degradation experiments demonstrated the biocompatibility *in vivo* of electrospinning fiber films with conductive coatings. The conductive NGCs combined with ES effectively facilitated nerve regeneration. The designed porous aligned NGCs with conductive coatings exhibited suitable physicochemical properties and excellent biocompatibility, thereby significantly enhancing PNR when combined with ES. This combination of porous aligned NGCs with conductive coatings and ES holds great promise for applications in the field of PNR.

1. Introduction

Peripheral nerve injury (PNI) refers to damage occurring in the peripheral nerve plexus, nerve trunk, or its branches, typically resulting from traumatic factors such as lacerations, motor vehicle accidents, compression injuries, and excessive stretching [1]. The management of long-distance (over 5 cm) nerve defects poses a significant surgical challenge due to the inability to directly suture nerves [2]. The current treatment for long-distance nerve defects is autologous nerve transplantation (ANT) [3]. However, ANT has several inherent disadvantages, including limited availability of donors, functional loss in the donor region, formation of neuromas, and mismatched nerve diameters [4]. To overcome these limitations, a tissue-engineered nerve guide conduit (NGC) was developed [5]. The NGC effectively isolates the regenerated nerve axon from surrounding scar tissue, therefore preventing compression of the nerve by adjacent tissues [6]. Additionally, the NGC plays a crucial role in accurately directing nascent neural tissue towards its intended target organ [7].

Various techniques were employed for the fabrication of NGCs, including freeze-drying, solvent casting, phase separation, gas foaming, three-dimensional (3D) printing, and electrospinning [8]. Electrospinning is an electrostatically driven process utilized to produce random or aligned fibers with diameters ranging from nanometers to microns [9]. The desired morphology of electrospinning fiber was achieved by adjusting process parameters, environmental conditions, and solution properties [5]. Many previous studies have demonstrated the indispensability of electrospinning fibers with aligned porous morphology for nerve regeneration, as they effectively enhance neuronal cell adhesion, proliferation, and guided growth while also modulating cytokine expression to a moderate extent [10,11]. Zamani et al. found that electrospinning poly(lactic-*co*-glycolic acid) (PLGA)

* Corresponding authorDepartment of Hand and Foot Surgery, Orthopedics Center, The First Hospital of Jilin University, Changchun, 130021, China.
** Corresponding author
E-mail addresses: zhaolir@jlu.edu.cn (L. Zhao), l_bin@jlu.edu.cn (B. Liu).

https://doi.org/10.1016/j.mtbio.2024.101064
Received 1 February 2024; Received in revised form 4 April 2024; Accepted 15 April 2024
Available online 18 April 2024

List of abbreviations

3D	Three-dimensional
AChE	Acetyl cholinesterase
ANT	Autologous nerve transplantation
ATP	Adenosine triphosphate
CCK-8	Cell counting kit-8
CLSM	Confocal laser scanning microscope
CMAPs	Compound muscle action potentials
CNS	Central nervous system
CPs	Conducting polymers
DAPI	4′,6-diamidino-2-phenylindole
DCM	Dichloromethane
DEG	Differentially expressed genes
DMEM	Dulbecco's modified eagle medium
DMF	Dimethylformamide
DMSO	Dimethyl sulfoxide
ECM	Extracellular matrix
EDX	Energy dispersive X-Ray
ELISA	Enzyme linked immunosorbent assay
ES	Electrical stimulation
FDA	Food and drug administration
FTIR	Fourier transform infrared
GFAP	Glial fibrillary acidic protein
GM	Gastrocnemius muscle
GO	Gene ontology
GSEA	Gene set enrichment analysis
H&E	Hematoxylin-eosin
IL-10	Interleukin-10
IT	Intermediary toe
KEGG	Kyoto encyclopedia of genes and genomes
MAP-2	Microtubule association protein-2
MAPK	Mitogen-activated protein kinase
MBP	Myelin basic protein
M-CSF	Macrophage stimulating factor
MEP	Motor endplate
NF200	Neurofilament-200
NGC	Nerve guide conduit
PANI	Polyaniline
PBS	Phosphate buffer saline
PC-12	Pheochromocytoma-12
PCL	Polycaprolactone
PEDOT	Poly(3,4-ethylenedioxythiophene)
PFA	Paraformaldehyde
PI	Propidium iodide
PL	Paw length
PLGA	Poly(lactic-*co*-glycolic acid)
PLLA	Poly(L-lactic acid)
PNI	Peripheral nerve injury
PNR	Peripheral nerve regeneration
PNS	Peripheral nervous system
PPy	Polypyrrole
PSS	Polystyrene sulfonate
ROS	Reactive oxygen species
RPMI-1640	Roswell park memorial institute-1640
SC	Schwann cell
SD	Sprague-Dawley
SEM	Scanning electron microscopy
SFI	Sciatic functional index
TCP	Tissue culture polystyrene
TEM	Transmission electron microscope
TNF-α	Tumor necrosis factor-α
TS	Toe spread
Tuj-1	Beta3-Tubulin
UVO	Ultraviolet ozone
XPS	X-ray photoelectron spectroscopy

porous cylindrical fibers significantly enhanced the attachment, growth, and proliferation of human A-172 nerve cells [12]. Filimona et al. validated that the surface porous topology of electrospinning film prevented microbial colonization and reduced the risk of postoperative infections, which is crucial in neural tissue engineering [13].

Although numerous previous studies have been conducted on the application of aligned electrospinning with surface porous morphology in neural tissue engineering, a majority of these studies solely focused on cellular experiments rather than validating their effects on neural regeneration in animal models. Zhang et al. demonstrated that the combination of aligned electrospinning NGCs and electrical stimulation (ES) effectively enhanced peripheral nerve regeneration (PNR), thereby suggesting that employing multiple treatment modalities may yield a favorable synergistic effect [14]. Due to its poor electrical conductivity, PLGA requires modification with a conductive coating to enhance neurostimulation by ES. Among the various options available, poly(3,4-ethylenedioxythiophene) (PEDOT) stands out as the most extensively studied polythiophene derivative due to its superior electrochemical stability, enhanced conductivity, and improved thermal stability compared to polypyrrole (PPy) and polyaniline (PANI) [15]. Unlike other conductive polymers, PEDOT doped with polystyrene sulfonate (PSS) can be easily dispersed in aqueous solution while maintaining excellent conductivity [16]. Therefore, the utilization of PEDOT:PSS represents a promising approach for developing conductive scaffolds that facilitate cell adhesion and promote cellular growth and differentiation [17].

The process of PNR is intricate, and achieving satisfactory therapeutic outcomes with a single material, scaffold, or treatment proves challenging. Henceforth, the future research direction should focus on composite treatments involving multiple materials or approaches [18]. Prabhakaran et al. suggested that the combination of ES with topographical cues synergistically promoted axonal growth, surpassing the effects of monotherapy [19]. In another study, agarose NGCs were combined with a PEDOT conductive coating to enhance their mechanical properties and significantly improve conductivity. Although ES was not applied in the experiment, the desired nerve repair effect was achieved, leading to the successful restoration of motor function in the lower limbs of rats [18]. Other studies have primarily focused on utilizing topographic cues or ES to influence schwann cell (SC) migration [20,21]. However, there is a scarcity of reports regarding the combination of ES, topographic cues, surface topography, and conductive coatings for PNR.

Here, the electrospinning fibers were integrated with optimized porous alignment and highly conductive materials, in conjunction with ES, to regulate nerve cell behavior and facilitate neural repair *in vivo*, as illustrated in Scheme 1. We fabricated aligned PLGA fibers and investigated the optimal preparation conditions for their surface porous morphology by varying solvent ratios. Considering the cytotoxicity of high concentrations of PEDOT:PSS solutions, we systematically explored gradient dilution to achieve an optimal concentration of conductive coatings that would provide good conductivity without compromising biocompatibility for the electrospinning fibers. The resulting composite NGCs exhibited significantly enhanced nerve regeneration in rats under ES, offering a facile approach to obtain a well-suited NGC for nerve tissue engineering applications in PNI.

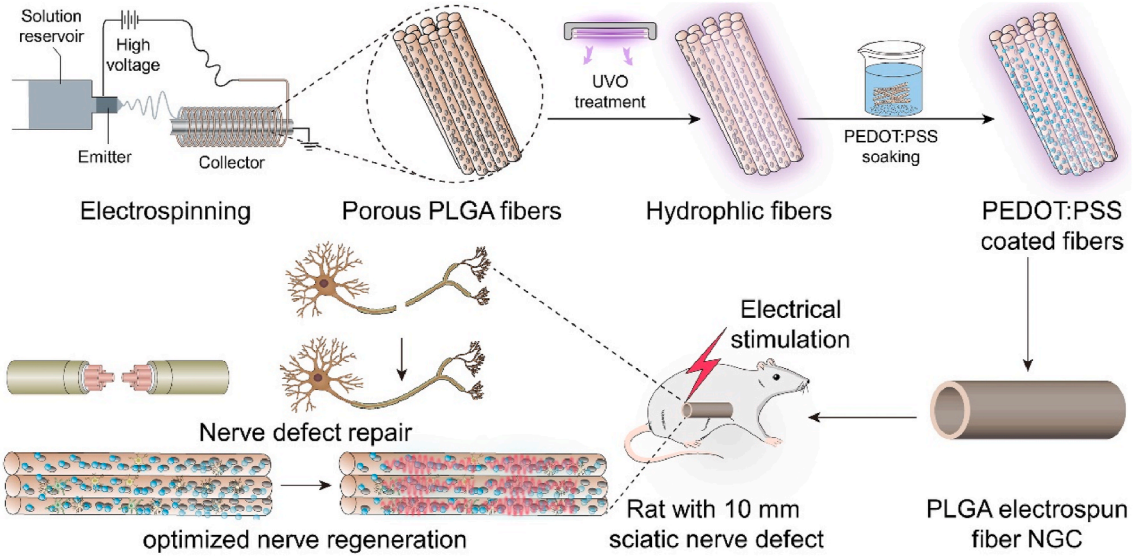

Scheme 1. Schematic illustration of porous aligned PEDOT:PSS-coated PLGA electrospinning NGC for promoting nerve regeneration under ES.

2. Materials and methods

2.1. Materials

PLGA ((LA): (GA) = 75:25; the molecular weight was 8×10^4 g mol^{-1}) was provided by Changchun SinoBiomaterials Co., Ltd (Changchun, P. R. China). Dimethylformamide (DMF, 0.948 g cm^{-3}) was purchased from Energy Chemical Co., Ltd (Shanghai, P. R. China). Dichloromethane (DCM, 1.325 g cm^{-3}) was purchased from XiLong Scientific Co., Ltd (Shenzhen, P. R. China). PEDOT:PSS, neurofilament-200 (NF200) antibody, glial fibrillary acidic protein (GFAP) antibody, and beta3-Tubulin (Tuj-1) antibody were purchased from Sigma-Aldrich (Shanghai, P. R. China). The rat hematoxylin-eosin (H&E) kit, the masson kit, the Roswell park memorial institute-1640 (RPMI-1640) medium, and the Dulbecco's modified eagle medium (DMEM) were purchased from Servicebio Co., Ltd (Wuhan, P. R. China). Cell counting kit-8 (CCK-8) was purchased from Beyotime Biotechnology Co., Ltd (Shanghai, P. R. China). 4′,6-diamidino-2-phenylindole (DAPI) was purchased from Solarbio Co., Ltd (Beijing, P. R. China). Phalloidin-FITC conjugate kit was purchased from Thermo Fisher Scientific Co., Ltd (Shanghai, P. R. China). Clear tissue culture polystyrene (TCP) plates were purchased from Corning Costar Co., Ltd (Cambridge, MA, USA). The living/dead cell double staining kit and acetylcholinesterase staining kit were purchased from Bestbio Co., Ltd (Shanghai, P. R. China). Myelin basic protein (MBP) antibody, rat pheochromocytoma-12 (PC-12) cells, and rat SCs were purchased from Bihe Biochemical Technology Co., Ltd (Shanghai, P. R. China). Sprague-Dawley (SD) rats were purchased from the animal experiment center of Jilin University (Changchun, P. R. China). Collagenase IV and DNase I were purchased from Sigma-Aldrich (Shanghai, P. R. China). Antibodies of CD11b, CD86, and CD206 were purchased from eBioscience Co., Ltd (Santiago, USA). Intracellular staining buffer was purchased from BIOCREATIVE Co., Ltd (Beijing, P. R. China). Enzyme linked immunosorbent assay (ELISA) kits were purchased from Servicebio Co., Ltd (Wuhan, P. R. China). RNA nano 6000 assay kit of the bioanalyzer 2100 system was purchased from Agilent Technologies Co., Ltd (CA, USA). Acetyl cholinesterase (AChE) kits were purchased from Bestbio Co., Ltd (Nanjing, P. R. China).

2.2. Preparation and characterization of PLGA electrospinning fibers under varying roller receiver speeds

2.52 g PLGA was dissolved in a mixture of 10 mL DMF and 10 mL DCM (10 wt%). The mixture was stirred for over 12 h until no undissolved PLGA particles were visible. Subsequently, the PLGA solution was aspirated into a 1 mL syringe under a device voltage of 14 kV and with a distance of 15 cm between the needle tip and the roller collector encapsulated in copper foil. The resulting electrospinning fibers obtained at different roller receiver speeds (0 rpm, 500 rpm, 1000 rpm, 1500 rpm, 2000 rpm, and 2500 rpm) were named as follows: PLGA-0, PLGA-500, PLGA-1000, PLGA-1500, PLGA-2000, and PLGA-2500, respectively. Scanning electron microscopy (SEM, Inspect-F50, FEI, Eindhoven, Finland) was employed to observe the alignment and surface morphology characteristics of the electrospinning fibers. Additionally, hydrophilicity characterization of the PLGA fibers was conducted by measuring their water contact angle using a contact angle meter (KRUSS, Hamburg, Germany).

2.3. Preparation and characterization of porous PLGA fibers with varying ratios of DCM and DMF blends

The PLGA was dissolved using varying ratios of DCM mixed with DMF, as indicated in Table 1, all for a 10 wt% PLGA solution.

We employed SEM to conduct morphological characterization of PLGA fibers. The densities and porosities were determined using the liquid phase displacement technique with ethanol as the displacing agent. To enhance hydrophilicity, the PLGA fiber films underwent a 50s treatment with an ultraviolet ozone (UVO) cleaner (42–220, Jelight, USA). The quality of the fiber film was M, followed by immersion in ethanol (volume V1) for 5 min, resulting in a total volume of ethanol and film denoted as V2. After removing the fiber film from ethanol, the remaining volume of ethanol was measured as V3. Subsequently, equation (1) was utilized to calculate the density (ρ) of the fiber film.

Table 1
Various ratios of DCM and DMF were utilized to dissolve PLGA for the preparation of electrospinning fibers.

The solvent's volume ratio	DCM	DMF	PLGA
12:1	3 mL	0.25 mL	0.47 g
10:1	3 mL	0.3 mL	0.47 g
8:1	3 mL	0.38 mL	0.48 g
6:1	3 mL	0.5 mL	0.49 g
4:1	2.6 mL	0.65 mL	0.45 g
3:1	2.4 mL	0.8 mL	0.44 g
2:1	2.2 mL	1.1 mL	0.44 g

$$\rho = \frac{M}{V2 - V3} \quad (1)$$

where M was in "g", and V2 and V3 were in "mL".

The porosity (ε) of the fiber film was determined using equation (2):

$$\varepsilon = \frac{V1 - V3}{V2 - V3} \quad (2)$$

where V1, V2, and V3 were in "mL".

We determined the water absorption of the fiber film with an initial mass of M0. The fiber films were immersed in deionized water for 24 h. After being removed from the water, excess moisture on the surface of the fiber films was absorbed using filter paper, and its quality was measured as M1. PLGA fiber films were subjected to vacuum drying at 40 °C for 24 h and then weighed as M2. The water absorption (δ) of the fiber film was calculated using equation (3):

$$\delta = \frac{M1 - M2}{M0} \quad (3)$$

M0, M1, and M2 were in "g".

2.4. The impact of PEDOT:PSS-coated porous PLGA fibers on cellular proliferation

To coat the porous PLGA fibers, we employed the PEDOT:PSS solution. Previous research has indicated that incorporating propanol or dimethyl sulfoxide (DMSO) into the PEDOT:PSS solution enhances its solubility and conductivity [22]. However, the use of organic solvents may potentially harm the mechanical properties and surface morphology of PLGA fiber films. Therefore, we chose to mix an equal volume of deionized water with PEDOT:PSS to avoid any potential damage. The UVO-treated fiber films were immersed in aqueous PEDOT:PSS solution for 1 h, dried under vacuum at 30 °C for 3 h, and subsequently rinsed with deionized water to eliminate any residual PEDOT:PSS from the surface [22].

With the PLGA fiber films, both coated and uncoated, placed in 96-well plates, we added 5×10^3 PC-12 cells suspended in 200 μL of RPMI-1640 medium to each well. Following a 24 h incubation period, the cell culture medium was aspirated and replaced with a mixture of CCK-8 reagent (dissolved at a concentration of 5 mg mL^{-1}) in serum-free medium at a ratio of 1:10. Subsequently, 100 μL of the mixture was added to each well and further incubated until an orange color developed. Proliferation rates were assessed using the Bio-Rad microplate detector (Bio-Rad 550, Hercules, California, USA). Cell experiments were conducted at both the 48 h and 72 h time points following previously described methods.

2.5. The exploration of the optimal coating concentration for PEDOT:PSS

We employed gradient dilution to explore the optimal coating concentration of PEDOT:PSS using rat PC-12 cells and SC cells for experiments. A total of 50 wells arranged in 5 rows and 10 columns were selected on a 96-well plate. Subsequently, each well was supplemented with 5×10^3 PC-12 cells and 200 μL of culture medium, followed by incubation for 24 h. The cell culture medium was then aspirated from each well, after which the leftmost five wells received an addition of 100 μL of PEDOT:PSS solution. Next, these wells were mixed thoroughly with an additional supplementation of 100 μL of cell culture medium before transferring a volume of 100 μL from this mixture into the second column's 5 wells. This process was repeated by adding another 100 μL cell culture medium and thorough mixing before pipetting the resulting mixture into the third column's wells for further dilution. This sequential procedure continued until reaching the tenth column where a final volume of well-mixed liquid measuring at 200 μL was obtained, discarding the 100 μL mixture.

After incubation for 24 h, the mixture was removed, followed by the addition of a mixture containing CCK-8 reagent solution and cell culture medium. The resulting mixture was further incubated until an orange color developed and subsequently analyzed using a microplate reader.

2.6. Preparation and characterization of porous PLGA fiber films coated with the optimal concentration of PEDOT:PSS

The porous PLGA fiber films were coated with PEDOT:PSS solution at the optimal concentration for promoting cell proliferation. We employed a digital multimeter (DLX890C+, Delixi Group Co., Ltd, Zhejiang, China) to determine the electrical conductivity of the PLGA fiber films. The cross-sectional area of the fiber film was determined by measuring its width and thickness using vernier calipers, and the conductivity (σ) was calculated based on equation (4):

$$\sigma = \frac{L}{AR} \quad (4)$$

R was the resistance of the fiber film in "MΩ"; L was the distance between the two electrodes in "cm"; A was the cross-sectional area of the fiber film in "cm^2".

We examined the surface morphology of PLGA fiber films after PEDOT:PSS coating using SEM. The presence of the coating on the fiber films was studied through mapping and energy dispersive X-Ray (EDX) spectroscopy. X-ray photoelectron spectroscopy (XPS) was employed to analyze the elemental sulfur present on the surface of PLGA fiber films. The mechanical properties of PLGA fiber films were evaluated using a universal testing machine (Shimadzu, Kyoto, Japan). We conducted mechanical property tests on the fiber films in both parallel and perpendicular orientations to the fiber alignment, with the stress-strain curves providing us with the maximum tensile strength data. Fourier transform infrared (FTIR) spectroscopy (Bio-Red Win-IR, Bruker, Karlsruhe, Germany) was employed to analyze uncoated PLGA fiber films, PEDOT:PSS conductive coating, and coated PLGA fiber films. The hydrophilicity of the coated PLGA fiber films was evaluated by measuring their water contact angle.

2.7. The in vitro and in vivo degradation of porous PLGA fiber films coated with PEDOT:PSS

We prepared non-porous, porous, and coated porous PLGA fiber films for *in vitro* degradation experiments. The weight of each fiber film was accurately measured, followed by immersion in 1 % elastase at 37 °C. The fiber films were removed every 10 days for vacuum drying and subsequent weighing to determine the remaining weight as a percentage of the initial weight at each time point.

The rats were anesthetized with a 2 % solution of pentobarbital sodium through intraperitoneal injection, and subsequently, an "L" shaped incision was made on the dorsal region of each rat. Following the separation of the subcutaneous tissue using a mosquito hemostat, the fiber films were implanted into the subcutaneous fascial layer and secured in place with sutures. Local tissues were excised at 1, 2, and, 3 months post-implantation of the fiber films, and paraffin sections were prepared after fixation of the tissues using a 4 % paraformaldehyde (PFA) solution. The rats' weights were recorded every 10 days following implantation.

2.8. The impact of PLGA fiber films with a coated porous surface on cellular behavior

We conducted cellular experiments using SC and PC-12 cells and employed SEM to characterize the cell morphology on the surface of the fiber films. Additionally, we performed cytoskeleton staining to assess the impact of electrospinning fiber alignment on cell growth and morphology. Furthermore, we evaluated the toxicity of PEDOT:PSS on nerve cells through living/dead cell double staining.

The porous PLGA fiber films were coated with the optimal concentration of PEDOT:PSS solution. Subsequently, the coated porous PLGA

fiber films were placed in 24-well plates, and a small well containing 2 × 10^4 cells was prepared with the fiber film for subsequent incubation. Following aspiration of the medium, the PLGA fiber films were washed twice using phosphate buffer saline (PBS). The electrospinning fiber films were fixed using 4 % PFA for 30 min. Sequentially, ethanol at concentrations of 30 %, 50 %, 70 %, 80 %, 90 %, 95 %, and pure ethanol was added to dehydrate the cells adhering to the PLGA fiber films for 30 min before their morphology was characterized using SEM.

The coated porous PLGA fiber films were placed into a 24-well plate, and 1 × 10^4 cells were seeded into each well of the plate and incubated. After removing the medium and rinsing the fiber films with PBS, the films were fixed with PFA. Following removal of PFA and rinsing of the fiber film with PBS, acetone at −20 °C was added for 5 min. The acetone was aspirated and the film was rinsed with PBS. Subsequently, the fiber film was stained using a phalloidin solution for 90 min, followed by 3 times rinses with PBS. Next, the fiber films were stained with a DAPI solution for 10 min and again rinsed 3 times with PBS. Finally, the stained cells were captured using a confocal laser scanning microscope (CLSM, T-PMT, Zeiss, Japan).

A sterile coverslip was placed on the bottom of a 6-well plate, and 2 × 10^5 cells along with 3 mL of cell culture medium mixed with the PEDOT:PSS solution were added into each well. The plate was then incubated for 48 h. Live cells were stained using calcein AM, while dead cells were stained using propidium iodide (PI). The coverslip was carefully lifted from the bottom of the 6-well plate and placed upside down onto a slide, which was subsequently captured using a fluorescence microscope (ECLIPSE C1, Nikon, Japan).

To assess the impact of electrospinning fibers on macrophages at the PNR sites, we employed ELISA to study cytokine secretion. Rat macrophages were cultured on electrospinning fibers, and cell supernatants were collected after 24, 48, and 72 h. The concentrations of tumor necrosis factor-α (TNF-α) and interleukin-10 (IL-10) in the supernatants were quantified using ELISA kits.

2.9. The procedures of animal experimentation

The female SD rats, weighing 220–250 g and aged 4–6 weeks, were provided with adequate water and food. All animals underwent a two-week acclimatization period before the animal experiments. A 10 mm sciatic nerve defect model was created to study the efficacy of coated aligned porous NGC combined with ES in promoting sciatic nerve regeneration in rats. The rats were randomly divided into 6 groups, each consisting of 10 individuals: nerve defect group, PLGA-1500 group, porous PLGA-1500 group, coated porous PLGA-1500 group, coated porous PLGA-1500 + ES group, and autograft group. After administering ether inhalation anesthesia to rats, a 2 % solution of pentobarbital sodium was intraperitoneally administered at a dosage of 2 mL kg^{-1} body weight. Once the anesthesia took effect, a longitudinal incision was made along the posterior aspect of the left femur to expose the sciatic nerve by gently separating the muscle tissue. The sciatic nerve was surgically resected to create a 10 mm nerve defect, and the area of the nerve defect was implanted with the NGC made of PLGA fiber film. In the autograft group, the resected nerve segments were utilized to bridge the nerve gaps after inversion, and each rat received an intramuscular injection of 80,000 units of penicillin post-surgery for infection prevention.

A Rigol DG1022 signal generator (Puyuan Jingdian Technology Co. LTD, Beijing, China) was utilized to administer ES treatment on rats in the postoperative ES group every other day for a total of 5 sessions. Following previous research findings, we configured the stimulation parameters to include a frequency of 20 Hz, a duty cycle of 50 %, and an operating voltage of 100 mV. Platinum wire electrodes were positioned within the proximal and distal tissues of the nerves, with each stimulation session lasting for 2 h [14]. The recovery progress of lower extremity nerves in rats was evaluated at both the 2-month and 3-month time points after treatment.

2.10. The analysis of walking tracks

To evaluate the recovery of the lower extremity function of rats, a walking track analysis was conducted on 5 rats from each group at 2 and 3 months post-treatment. A white paper was placed on the bottom of the plexiglass runway, while the hind feet and toes of the rats were blackened with the dye. A light source positioned at the end of the runway was utilized to stimulate forward movement in the rats, thereby leaving their footprints imprinted on the paper. The following parameters were obtained from the footprints of the rats: paw length (PL), which refers to the distance from hindfoot to distal middle toe; intermediary toe spread (IT), which represents the distance between the second and fourth toes; Toe spread (TS), indicating the distance between the first and fifth toes. The sciatic functional index (SFI) was calculated using formula (5):

$$SFI = \frac{-38.3 \times (EPL - NPL)}{NPL} + \frac{109.5 \times (ETS - NTS)}{NTS} + \frac{13.3 \times (EIT - NIT)}{NIT} - 8.8 \quad (5)$$

where E denoted the left footprints, while N represented the right footprints.

2.11. Electrophysiological analysis of the sciatic nerve and characterization of implanted aligned electrospinning NGCs

The bilateral compound muscle action potentials (CMAPs) of the lower extremities in rats were recorded at 2 and 3 months post-treatment using a 9033A07 EMG/evoked potentiometer (Bendi Medical Equipment Co., Ltd, Shanghai, China). Following anesthesia induction, longitudinal incisions were made posterior to the femur to expose the nerve. The gastrocnemius muscle (GM) was penetrated by one recording electrode in a vertical manner, while another recording electrode was inserted vertically into the rat at the Achilles tendon. The grounding electrode was placed in the rat's tail, with the stimulation electrode positioned at the proximal region of the regenerated nerve. Pulses at 50 Hz were used to stimulate the sciatic nerves, and for each group, the amplitudes and latencies of CMAP were recorded. The electrospinning NGCs within the sciatic nerve defect area were extracted and subjected to vacuum drying, followed by SEM observation to assess fiber alignment.

2.12. Histological and immunofluorescence examination of the GM and regenerated sciatic nerve

We consulted the previous study for the current experimental section [14]. We assessed the histopathology of regenerated nerves and GM specimens from rats at 2 and 3 months post-treatment. The bilateral GMs of rats were measured in terms of weight, and the percentage of bilateral muscle weight was calculated using equation (6):

$$\text{Weight}\ (\%) = \frac{\text{Weight (E)}}{\text{Weight (N)}} \quad (6)$$

Weight (E) and Weight (N) denoted the muscle weight of the GM on the experimental and normal sides, respectively.

The GM and regenerated nerves were prepared, stained, and subsequently observed under a microscope (ECLIPSE C1, Nikon, Japan). The diameter of the regenerated nerve fibers and the thickness of myelin sheaths were characterized using a transmission electron microscope (TEM, HT7800/HT7700, hitachi, Japan). Immunofluorescence staining for NF200, MBP, GFAP, and Tuj-1 was performed to detect neural axon regeneration, followed by image acquisition using CLSM. The diameters of GM fibers, regenerated nerve fibers, and myelin sheath thickness were quantified using nano measurer software (http://www.downxia.com) based on the image results. Additionally, the immunofluorescence results of the regenerated nerves were analyzed using ImageJ software

(http://rsb.info.nih.gov/ij/).

2.13. Immunocytometric analysis and transcriptomic assay were conducted on the regenerated sciatic nerve, while motor endplate (MEP) assay was performed on GM

After the administration of anesthesia, the rats were subjected to cardiac perfusion using a saline solution. The regenerated nerves were then extracted and diced into small fragments, which were subsequently placed in a digestion buffer containing RPMI-1640 medium, collagenase IV, and DNase I for 1 h. Following this step, the samples underwent filtration through a 70 μm nylon filter to eliminate any undigested debris, while cells were collected by centrifugation. Finally, the cells were stained with 1 μL of CD11b and CD86 antibodies for 30 min at 4 °C under light protection. After the completion of staining, the buffer was added to suspend the staining, and subsequent washing steps were performed. Following fixation with PFA and additional buffer washes, permeabilization was achieved using intracellular staining buffer. After further washing with buffer, cells were stained with 1 μL CD206 antibody for 40 min under light-protected conditions. Subsequently, after discontinuing the staining and performing a final round of cell washing using buffer, the samples were analyzed by flow cytometry (Becton, Dickinson and Company, USA).

The GM specimens were prepared as frozen sections, which were then immersed in pre-cooled 10 % calcium formaldehyde for 10 min. Subsequently, the sections were thoroughly rinsed with distilled water. Following this, the sections were incubated in an AChE incubation solution at 37 °C for 2 h, ensuring they were kept away from light until they attained a light brown coloration. The sections underwent further rinsing under running water and subsequently underwent staining with hematoxylin stain for 5 min. This was followed by another round of rinsing under running water lasting for 10 min. Finally, after routine sealing procedures had been carried out, photographs were captured using the microscope (ECLIPSE C1, Nikon, Japan).

The animal tissue specimens were cryopreserved at −80 °C immediately after isolation for optimal preservation. RNA integrity was evaluated using the Bioanalyzer 2100 system with the RNA nano 6000 assay kit. Total RNA was utilized as input material for the preparation of RNA samples. The index-coded samples were clustered on a cBot cluster generation system using TruSeq PE cluster kit v3-cBot-HS (Illumia), following the manufacturer's instructions. After cluster generation, the library preparations were sequenced using an Illumina Novaseq platform, resulting in the generation of 150 bp paired-end reads. The raw data (raw reads) in fastq format underwent initial processing through fastp software. Reference genome and gene model annotation files were directly downloaded from the genome website. The mapped reads for each sample were assembled using StringTie (v1.3.3b) in a reference-based approach [23]. Featurecounts v1.5.0-p3 was employed to quantify the number of reads mapped to each gene.

The clusterProfiler package was utilized to perform Gene ontology (GO) enrichment analysis on differentially expressed genes (DEG), with gene length bias correction applied. GO terms exhibiting corrected P-values less than 0.05 were deemed significantly enriched by DEG. The kyoto encyclopedia of genes and genomes (KEGG) serves as a database resource for understanding high-level functions and utilities of biological systems, including cells, organisms, and ecosystems, based on molecular-level information derived from large-scale molecular datasets generated through genome sequencing and other high-throughput experimental technologies (http://www.genome.jp/kegg/). We utilized the clusterProfiler package to assess the statistical enrichment of differential expression genes in KEGG pathways. Gene set enrichment analysis (GSEA) is a computational approach employed to determine if a predefined gene set exhibits significant and consistent differences between two biological states. The GSEA analysis tool (http://www.broadinstitute.org/gsea/index.jsp), along with GO and KEGG datasets, were independently employed for conducting GSEA.

2.14. The assessment of nutritional status and the testing of organ toxicity in rats

The nutritional status of the rats was evaluated based on changes in body weight over 3 months. The heart, liver, spleen, lung, and kidney specimens were fixed in PFA solution, followed by dehydration and preparation of paraffin sections. These sections were then deparaffinized and rehydrated by using xylene immersion. Subsequently, all slices were stained with H&E dye, rinsed with water, and dehydrated using graded ethanol. Finally, the sections underwent two rounds of xylene soaking before capturing photomicrographs using the microscope (ECLIPSE C1, Nikon, Japan).

2.15. Statistical analysis

Data were presented as the mean ± standard deviation (SD) and were analyzed with the GraphPad Prism 7.04 software (Graphpad Inc., San Diego, CA, USA). The Student's t-test was used for statistical analysis. Statistical significance was set at $^{*}P < 0.05$ and high statistical significance was set as $^{**}P < 0.01$ and $^{***}P < 0.001$.

3. Results and discussion

3.1. The PLGA electrospinning fibers were prepared using various roller receiver speeds

In the study of electrospinning fiber alignment, a solution was prepared using equal volume ratios of DCM and DMF. Due to its high volatility, an excessive amount of DCM can lead to rapid viscosity increase in the solution, resulting in clogging of the jet needle and failure in the preparation process. Conversely, an excessive proportion of DMF may generate numerous beaded fibers that adversely affect the surface morphologies of the fibers. Therefore, for our study on electrospinning fiber alignment, we opted to mix these two solutions in equal volumes and successfully obtained PLGA fibers with uniform morphology and excellent alignment (Fig. 1A).

The alignment of the electrospinning fibers is influenced by the type of receiver employed. Isotropic electrospinning fibers are obtained when a plane receiver is utilized, whereas anisotropic fibers are achieved with a roller collector. The impact of rotational speed on fiber alignment was analyzed through SEM images at a magnification of 5×10^3. The fibers exhibited an isotropic morphology when a plane collector (0 rpm) was utilized, as depicted in Fig. 1A. However, the alignment of the fibers was limited when a roller collector operated at a lower speed (500 rpm). As the roller speed increased, so did the alignment of fibers. Nevertheless, once the speed surpassed a critical value, further increments resulted in diminished fiber alignment. The continuous centrifugal and shear force generated by the high-speed roller collector resulted in the fibers being easily pulled in different directions, thereby diminishing their overall alignment [24]. Utilizing a methodology employed in previous studies, we determined that the alignment of PLGA fibers at 500 rpm, 1000 rpm, 1500 rpm, 2000 rpm, and 2500 rpm was calculated to be 45 %, 66 %, 77 %, 71 %, and 74 % respectively [25] (Fig. 1B).

The water contact angles of the PLGA fiber films prepared at different roller receiver speeds were shown in Fig. 1D, exhibiting values of 123.51 ± 0.98°, 123.58 ± 1.61°, 122.21 ± 2.32°, 118.63 ± 2.49°, 120.62 ± 2.14°, and 117.71 ± 1.62° (Fig. 1E). These results consistently demonstrated the hydrophobic nature of all PLGA fiber films fabricated in our study. The diameters of the isotropic PLGA fibers measured 0.67 ± 0.02 μm (Fig. 1F). The electrospinning fibers prepared using the roller receiver exhibited significantly smaller diameters compared to the isotropic fibers, which can be attributed to fiber stretching induced by the centrifugal force generated through rotation of the roller receiver [26].

In addition to the rotational speed of the receiver, the diameter of the electrospinning fibers is closely correlated with other preparation

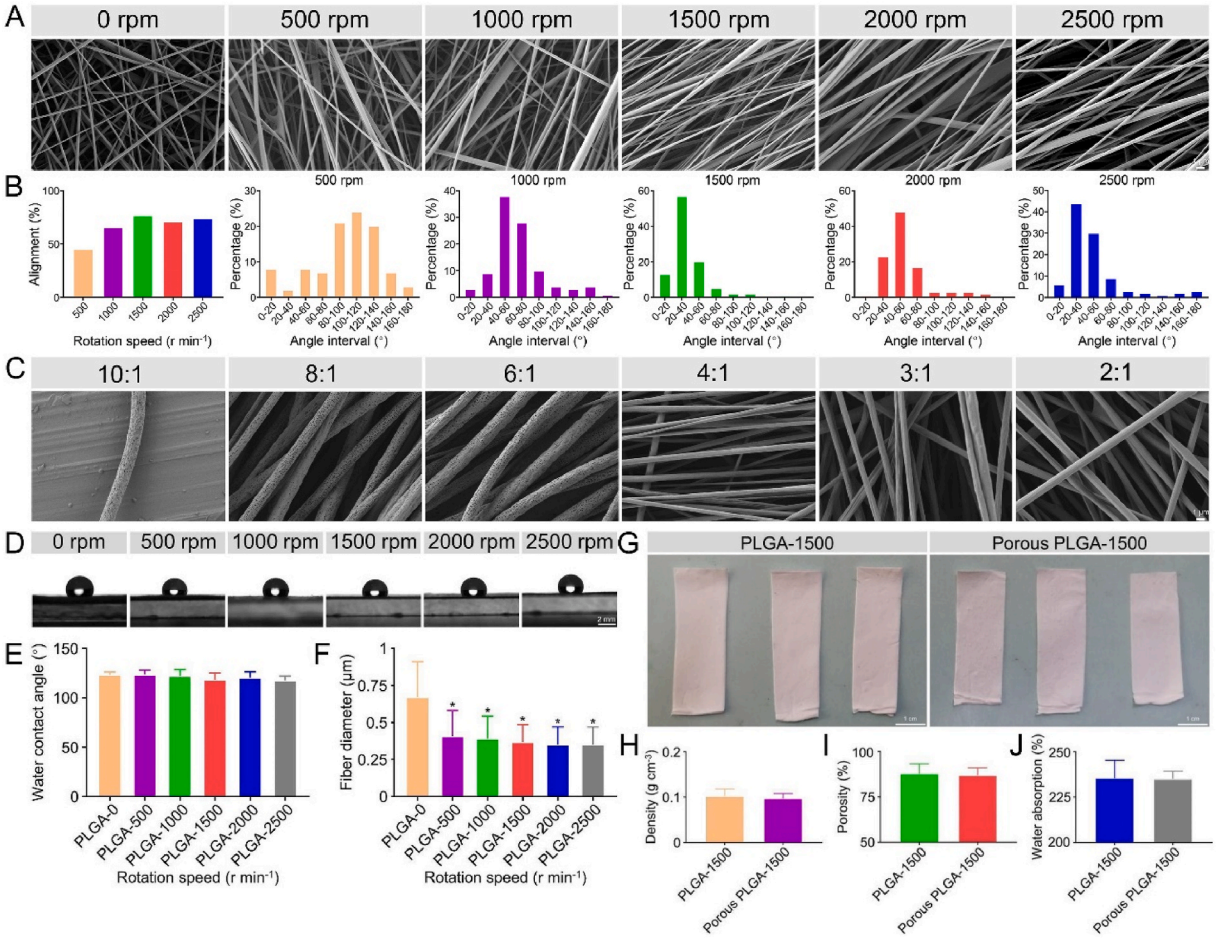

Fig. 1. Preparation of aligned porous electrospinning fibers and their physical properties. (**A**) SEM images depict PLGA fibers at various roller speeds. (**B**) The alignment of PLGA fibers is quantified at different rotational speeds (n = 100, n represents the number of electrospinning fibers for each speed). (**C**) SEM images display PLGA electrospinning fibers prepared using different volume ratios of DCM/DMF polymer solutions. (**D**) and (**E**) The hydrophilicity of PLGA fiber films with different alignments is evaluated (n = 7, n indicates the number of samples tested in each group). (**F**) Fiber diameter measurements are conducted on PLGA fiber films at different roller speeds to assess their size distribution and uniformity (n = 100, n represents the number of electrospinning fibers for each rotational speed; * indicates $P < 0.05$ compared with PLGA-0 group). (**G**) External phase, (**H**) density, (**I**) porosity, and (**J**) water absorption of different PLGA fiber films (n = 3, n indicates the number of samples tested in each group). All statistical data are represented as mean ± SD.

parameters. Ramacciotti et al. demonstrated that an increase in polymer solution concentration resulted in a corresponding enlargement of fiber diameter, potentially attributed to the higher viscosity of concentrated solutions and slower formation of Taylor's cone, necessitating a stronger electric field force for electrospinning fiber preparation [27]. The electric field force was enhanced by increasing the applied voltage, resulting in a decrease in the diameter of the prepared fibers. It was observed that higher voltages led to smaller fiber diameters. Other preparation parameters, such as temperature, humidity, and the distance between the jetting needle and receiver, had minimal impact on electrospinning fiber diameter [27]. The previous study demonstrated a direct correlation between the velocity of polymer solution spraying and the resulting fiber diameter, potentially attributed to reduced stretching time under the influence of an electric field. The inadequate stretching was identified as a contributing factor for larger fiber diameters [28].

3.2. The porous PLGA fibers were fabricated by blending varying ratios of DCM and DMF

We fabricated electrospinning fibers with a rough, porous surface structure using a phase separation method (Fig. 1C). PLGA particles were dissolved in a mixture of DCM and DMF at varying volume ratios (10:1, 8:1, 6:1, 4:1, 3:1, 2:1). The presence of porous structures was attributed to the solvent evaporation rate during fiber preparation. The formation of porous structures in PLGA fibers was facilitated by a higher percentage of volatile DCM in the solvent. However, if the DCM ratio exceeded 8:1, severe clogging occurred at the injection port and only a few PLGA fibers could reach the roller receiver. Increasing the DMF ratio beyond a certain level resulted in the disappearance of the porous structure and the development of a banded groove structure on the fiber surface (at ratios of 4:1 and 3:1), which may be attributed to insufficient volatility of the solvent to form the porous structure by liquid phase separation. As the DMF ratio continued to increase, the banded grooves on the fiber surface gradually disappeared and were replaced by a smooth surface (2:1). In order to achieve the optimal structure of PLGA fibers, we ultimately selected a 6:1 ratio for fiber preparation.

Porous fibers are of interest for various applications, such as filtration or tissue engineering repair [29]. For instance, specific surface topologies play a crucial role in influencing cell behavior and facilitating specific adsorption processes. Bognitzki et al. have concluded that the selection of appropriate parameters and solvents during electrospinning can directly yield porous fibers [30]. The porous morphology of the fibers is achieved through phase separation during the electrospinning process, resulting in spinodal or binodal types of phase morphologies within the fibers. This also leads to a rapid increase in the jet surface within a few milliseconds. Solvent evaporation occurs on time scales

significantly below the second-range, allowing for the crossing of phase boundaries and the formation of structures through phase separation [30].

The previous study revealed that the utilization of volatile solvents, such as DCM, resulted in the formation of polymer fibers with a regular porous structure. Their interpretation was that rapid phase separation during the electrospinning process led to the creation of a consistent phase morphology [30]. It appeared that solvent-rich regions transformed pores. Substituting DCM with a less volatile solvent notably diminished the propensity for pore formation, which aligned with our experimental findings.

The porous structure did not disrupt the structural guidance for neurons in the aligned fibers, as evidenced by numerous previous studies. For instance, Kim et al. demonstrated that fibrous scaffolds composed of porous and aligned polycaprolactone (PCL)/silk/quercetin exhibited superior nerve repair capabilities compared to aligned nerve scaffolds [31]. Additionally, Zhou et al. showed that elliptical nano-pore surfaces on aligned electrospinning poly(L-lactic acid) (PLLA) fibers enhanced the cellular response of vascular smooth muscle cells [32].

The fiber diameter tended to decrease as the percentage of DCM decreased, as depicted in Fig. 1C, aligning with previously reported findings [28]. We posit that the variation in the DCM ratio primarily influenced the surface morphology of the fibers rather than their diameter. Furthermore, the impact of fibers with different diameters on neuronal cells remained a subject of debate. Daud et al. concluded that thicker fibers exhibited promotion of nerve axon growth [28]. However, Yao et al. demonstrated no significant variance in the promotion of axon growth by fibers with different diameters [33]. It is noteworthy that the morphology of electrospinning fibers is influenced by various factors, including diverse polymers and solvent ratios. In our preparation process, when the ratio of DCM to DMF was 12:1, the highly volatile DCM rapidly evaporated and led to a rapid increase in solution viscosity. Consequently, the formation of Taylor's cone was delayed due to the increased viscosity, resulting in solidification and blockage of the injection needle. This phenomenon was also observed at a ratio of 10:1.

As shown in Fig. 1G, the porous PLGA fiber films were prepared using a mixed solution of DCM/DMF (V:V = 6:1), and their appearance resembled that of the nonporous PLGA fiber films. The densities of the nonporous and porous fiber films were calculated to be 0.10 ± 0.01 g cm^{-3} and 0.09 ± 0.01 g cm^{-3}, respectively. There was no significant difference in densities observed between the two types of fiber films, possibly due to the minimal impact of the nanoscale porous structure on their densities (Fig. 1H).

The porosity of nonporous and porous PLGA fiber films was determined using the ethanol displacement technique, yielding values of 87.91 ± 3.11 % and 86.93 ± 2.43 %, respectively. The inability of ethanol to penetrate nanoscale pores can be attributed to its surface tension. Given that both fiber films were prepared under identical rotational speed, their alignments were similar, resulting in comparable porosities (Fig. 1I). The water absorption capacities of the nonporous and porous PLGA films were 214.11 ± 2.32 % and 214.08 ± 0.96 %, respectively. However, due to their similar porosities, there was no significant difference observed in their water absorption rates (Fig. 1J).

3.3. The impact of PEDOT:PSS-coated porous PLGA fibers on cellular proliferation

Conducting polymers (CPs) are polymers with delocalized electrons in the backbone and whose backbone atoms are connected to π-bonds. The conjugated backbone provides a pathway for electron migration, resulting in enhanced electrical conductivity [22]. CPs are generally considered non-toxic and have no impact on cell growth [34]. Numerous CPs have been utilized in the field of tissue engineering, including PPy, PANI, PEDOT, and poly(3-hexylthiophene) [22]. The conducting polymer PEDOT is commonly doped with PSS to form a stable aqueous suspension of particles [35]. Due to its exceptional chemical stability and conductivity, PEDOT finds applications in diverse fields including energy reserves, sensors, conductor electrode materials, biotechnology, and medicine [36]. Ghasemi-Mobarakeh et al. reported that the incorporation of CPs in tissue engineering has been shown to enhance cell adhesion and proliferation [37]. Similarly, Shahini et al. achieved satisfactory outcomes by utilizing PEDOT:PSS in bone tissue engineering [38]. In this study, we employed the dip-coating technique to uniformly coat PLGA fiber films with PEDOT:PSS solution and investigated its impact on nerve cell growth (Fig. S1A).

We assessed the proliferation of PC-12 cells at various time points using the CCK-8 reagent. As seen in Fig. S1B, uncoated PLGA fiber films exhibited significant promotion of cell proliferation at 24h, 48h, and 72h, whereas coated fiber films demonstrated inhibition of cell proliferation ($P < 0.001$). The pre-treatment of both sets of PLGA fiber films with UVO enhanced their hydrophilicity, potentially facilitating cell adhesion and proliferation [39]. A previous study indicated that high concentrations of PEDOT:PSS solution may exhibit cytotoxicity [40]. Babaie et al. reported that lower concentrations of PEDOT:PSS solution can enhance cellular activity [41]. The conductivity of PEDOT:PSS facilitates cell signaling and promotes the adsorption of cell surface proteins [42]. Therefore, we planned to perform a gradient dilution of the PEDOT:PSS solution to study its optimal coating concentration.

3.4. Exploring the optimal coating concentration of PEDOT:PSS solution for coating

Our study investigated the impact of varying concentrations of PEDOT:PSS solution on cellular proliferation. The presence of a high-concentration solution significantly impeded cell growth; however, upon dilution, cells exhibited improved growth potential. We conducted a gradient dilution of the PEDOT:PSS solution using PBS (Fig. 2A). At a concentration of 0.55 wt%, no significant change in color was observed for the diluted PEDOT:PSS solution. As the concentration decreased to 0.017 wt%, the solution gradually lightened in color and approached transparency. Different concentrations of PEDOT:PSS solution were employed to assess their effects on PC-12 cell and SC proliferation.

The proliferation of both cells at different time points was assessed using CCK-8 reagent (Fig. 2B). Even when the PEDOT:PSS solution was diluted to a concentration of 0.138 wt%, the growth of PC-12 cells remained significantly inhibited after 24 h of incubation. However, when a solution with a concentration of 0.069 wt% was used in cell culture, the proliferation of the cells showed significant improvement while still exhibiting some degree of inhibition.

The cell proliferation in the 0.034 wt% solution exhibited further enhancement upon dilution of the coating solution. Subsequent dilutions did not yield significant differences in cell proliferation between neighboring concentrations, yet overall trends indicated a gradual increase in cell proliferation with solution dilution, followed by a decline after reaching a certain concentration. The proliferation of PC-12 cells at the time points of 48 and 72 h, as well as SCs, exhibited a similar pattern. This could be attributed to the impact of highly concentrated CP solution on cell growth and proliferation due to its permeability and toxicity, while the hydrophilic and conductive properties of PEDOT:PSS facilitated cell adhesion when the solution was appropriately diluted [43]. The CP can induce an electric field in the cell membrane, and this alteration of ion channels and bioelectricity within the membrane may further enhance cell proliferation [43]. Based on the experimental results from 6 time points, a solution concentration of 0.017 wt% was determined as the optimal concentration for promoting cell proliferation. Therefore, we selected this specific concentration to prepare the coated conduit.

3.5. The optimal concentration of PEDOT:PSS was used to coat porous PLGA fiber films

The majority of nerve tissue engineering research on PEDOT has

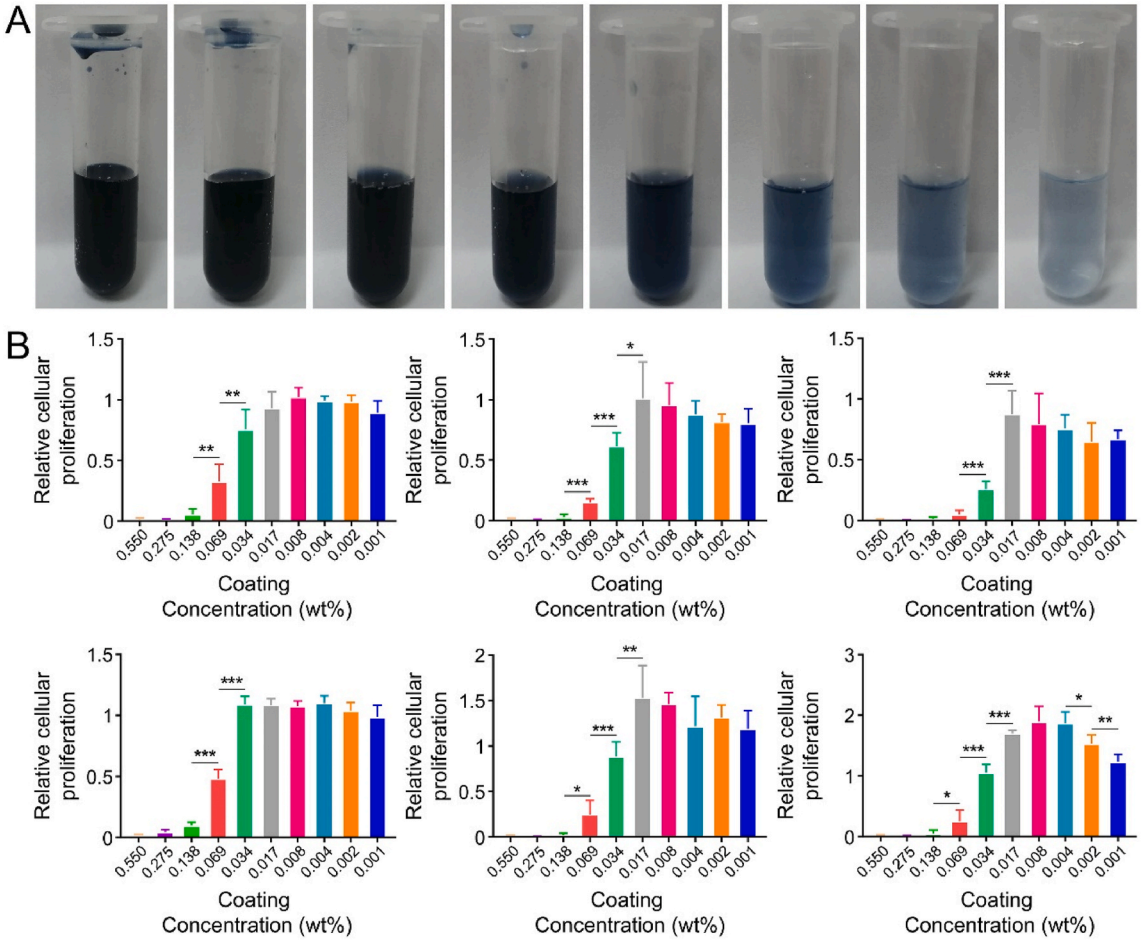

Fig. 2. The impact of gradient dilution of the PEDOT:PSS solution on cell proliferation. (**A**) The external phase of the gradient dilution of the PEDOT:PSS solution. (**B**) The impact of gradient dilution of the PEDOT:PSS solution on the proliferation of PC-12 and SC cells (n = 5, n represents the number of experimental replicates at each coating concentration). All statistical data are represented as mean ± SD (* indicates $P < 0.05$, ** indicates $P < 0.01$, *** indicates $P < 0.001$).

focused on its application as an electrode material. In contrast to PANI, PEDOT is soluble and can be chemically modified in various organic solvents, making it suitable for a wide range of implantable nerve scaffolds [44]. Additionally, PEDOT:PSS exhibits both ionic and electronic conductivity due to its porous nature, enabling the exchange of ions between the material and the biological medium. Although previous reports have suggested that PEDOT may degrade during ES, other studies have reported that PEDOT can be stabilized over approximately 100 million pulses using parameters matched to peripheral nervous system (PNS) [45]. Therefore, it is crucial to select an appropriate concentration of PEDOT:PSS coating for effective ES treatment in PNR.

The external phase of the PLGA fiber film, after being coated with the optimal concentration of PEDOT:PSS solution, is shown in Fig. 3A. The electrical conductivity of NGC also plays a crucial role in effectively promoting PNR [14]. As illustrated in Fig. 3B, the aligned fiber films exhibited anisotropic conductivity values of 0.07 ± 0.01 S cm^{-1} parallel to the fibers and 0.02 ± 0.01 S cm^{-1} perpendicular to the fibers ($p < 0.001$). This disparity can be attributed to the preferential movement of electrons along the fiber direction while hindering their movement perpendicular to it [46]. Zhang et al. demonstrated that the disparity in electrical conductivity between parallel and perpendicular orientations of electrospinning fibers was more than tenfold [14]. In contrast, our findings revealed that the discrepancy in conductivity between these two directions was less than fivefold, which can be attributed to the interconnection of adjacent fibers through the PEDOT:PSS coating, thereby reducing the variance in conductivity.

The SEM images of the porous PLGA fibers before and after coating with appropriate concentrations of PEDOT:PSS are presented in Fig. 3C and D, respectively. Before coating, the PLGA fibers exhibited a smooth surface except for the presence of porous structures. In contrast, the PEDOT:PSS coating did not cover the pores but was uniformly distributed on the fiber surface, providing an ideal foundation for nerve cell adhesion and proliferation. The coated PLGA fiber films were analyzed using mapping testing and EDX spectroscopy to detect the presence of sulfur elements (Fig. 3E). Elemental sulfur was exclusively found in the PEDOT:PSS coating, while no traces were observed in the PLGA film. Mapping testing results demonstrated a uniform distribution of conductive coatings on the surface of PLGA films, as evidenced by the presence of sulfur elements throughout. Additionally, EDX analysis confirmed the successful coating of the PLGA film surface with PEDOT:PSS.

To further investigate the conductive coating on the film, XPS testing was conducted on the coated film to analyze elemental sulfur. As shown in Fig. S2, the 2P binding energies of elemental sulfur in PSS and PEDOT were approximately 169 eV and 165 eV, respectively, which aligned with the previous research [47]. These findings additionally corroborated the presence of PEDOT:PSS conductive coatings on PLGA films.

The mechanical properties of the coated and uncoated fiber films were evaluated using an electronic universal testing machine (Fig. 3F). The stress-strain curve demonstrated that the uncoated PLGA fiber film exhibited favorable tensile properties, with its elastic response attributed to the excellent flexibility within the range of elastic deformation (Fig. 3G) [48]. Conversely, when subjected to stress-strain tests perpendicular to the fiber alignment, the samples easily detached due to

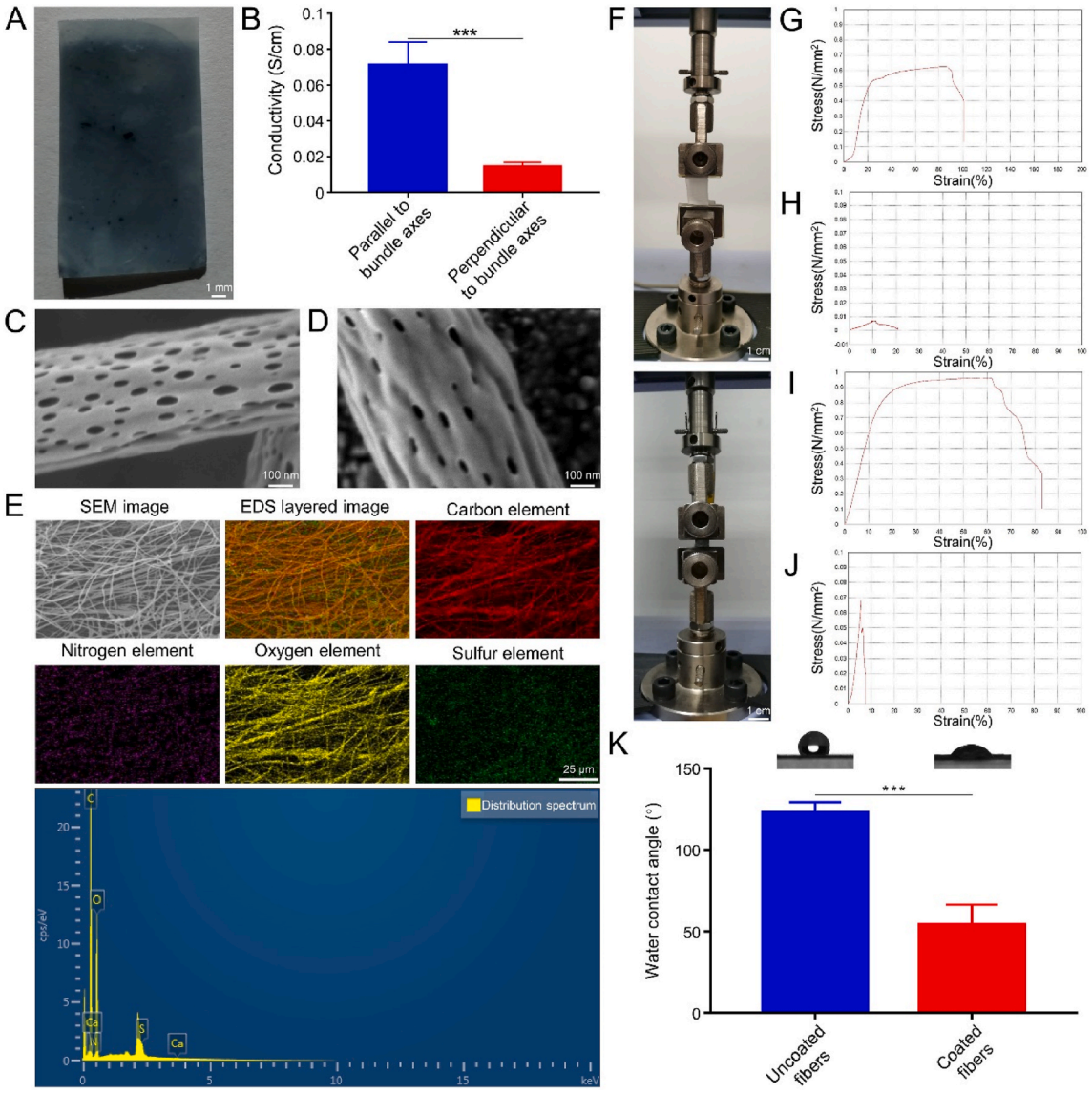

Fig. 3. External phase and characterization of porous PLGA electrospinning fibrous films coated with the optimal concentration of PEDOT:PSS. (**A**) The external phase of the coated porous PLGA electrospinning fiber film. (**B**) The electrical conductivity of coated porous PLGA electrospinning fiber films (n = 9, n represents the number of samples tested in each group). The surface morphology of (**C**) uncoated and (**D**) coated porous PLGA fiber films. (**E**) The mapping and EDX results of porous PLGA fiber films coated with optimal concentrations of PEDOT:PSS (n = 3, n indicates the number of samples tested in each group). (**F**) The mechanical properties of PLGA fiber films were tested. Stress-strain curves were obtained for uncoated PLGA fiber films in both parallel (**G**) and perpendicular (**H**) directions to the fiber alignment (n = 3, n indicates the number of samples tested in each group). Stress-strain curves were obtained for coated PLGA fiber films in both parallel (**I**) and perpendicular (**J**) directions to the fiber alignment (n = 3, n indicates the number of samples tested in each group). (**K**) The *in vitro* hydrophilicity of coated and uncoated PLGA fiber films (n = 10, n indicates the number of samples tested in each group). All statistical data are represented as mean ± SD (*** indicates $P < 0.001$).

a lack of opposing forces in the vertical direction caused by anisotropic electrospinning fibers (Fig. 3H).

The stress-strain curve obtained from tensile testing conducted parallel to the fiber direction on the coated fiber film is shown in Fig. 3I. Following the coating process, enhancements were observed in the tensile elastic limit, elastic modulus, and strength limit of the fiber film; however, a reduction was noted in its breaking elongation. The accumulation of conductive coating at the joints of different fibers may contribute to this phenomenon, as the adhesive nature of the coating impedes fiber elongation and sliding between them. Consequently, tensile strength increases while deformation capacity [49]. The change in mechanical properties of the coated film was observed not only parallel to the fiber alignment but also perpendicular (Fig. 3J). The increased viscosity of the conductive coating enhanced adhesion between fibers, increasing the tensile strength. However, it also heightened material brittleness and consequently decreased breaking elongation.

Although the porous structure has some impact on the mechanical properties of electrospinning fibers, the presence of a conductive coating enhances their mechanical strength. The elastic modulus of uncoated fiber film parallel to the fibers was 2.29 ± 0.15 MPa (Fig. 3G), whereas it increased to 5.33 ± 0.19 MPa after coating (Fig. 3I). These improved mechanical properties provide sufficient support for nerve regeneration [50].

The FTIR spectra of uncoated PLGA fiber film, PEDOT:PSS conductive coating and coated PLGA fiber film were presented in Fig. S3. The absorption peak (-OH) at both ends of PLGA was observed at 3509 cm^{-1}. Meanwhile, the stretching vibration peak (-C═O) of PLGA appeared at

1759 cm^{-1}, exclusively in the spectrum of PLGA and not in PEDOT:PSS. A distinctive peak (-SO_3) was detected at 1224 cm^{-1} solely in the PEDOT:PSS conductive coating but absent in the PLGA. The stretching vibration peak (–COO–) at 1174 cm^{-1} was observed exclusively in PLGA and not in PEDOT:PSS. Additionally, the characteristic peak (-C-*O*-C-) at 1094 cm^{-1} was identified solely in PEDOT:PSS. These findings from the FTIR spectra indicate the successful coating of PLGA fiber film with a conductive PEDOT:PSS coating.

The water contact angle serves as an indicator of the hydrophilicity of the electrospinning fiber film. A water contact angle exceeding 90° indicates its hydrophobic nature, whereas a value below 90° suggests acceptable hydrophilicity [22]. While hydrophilicity plays a crucial role

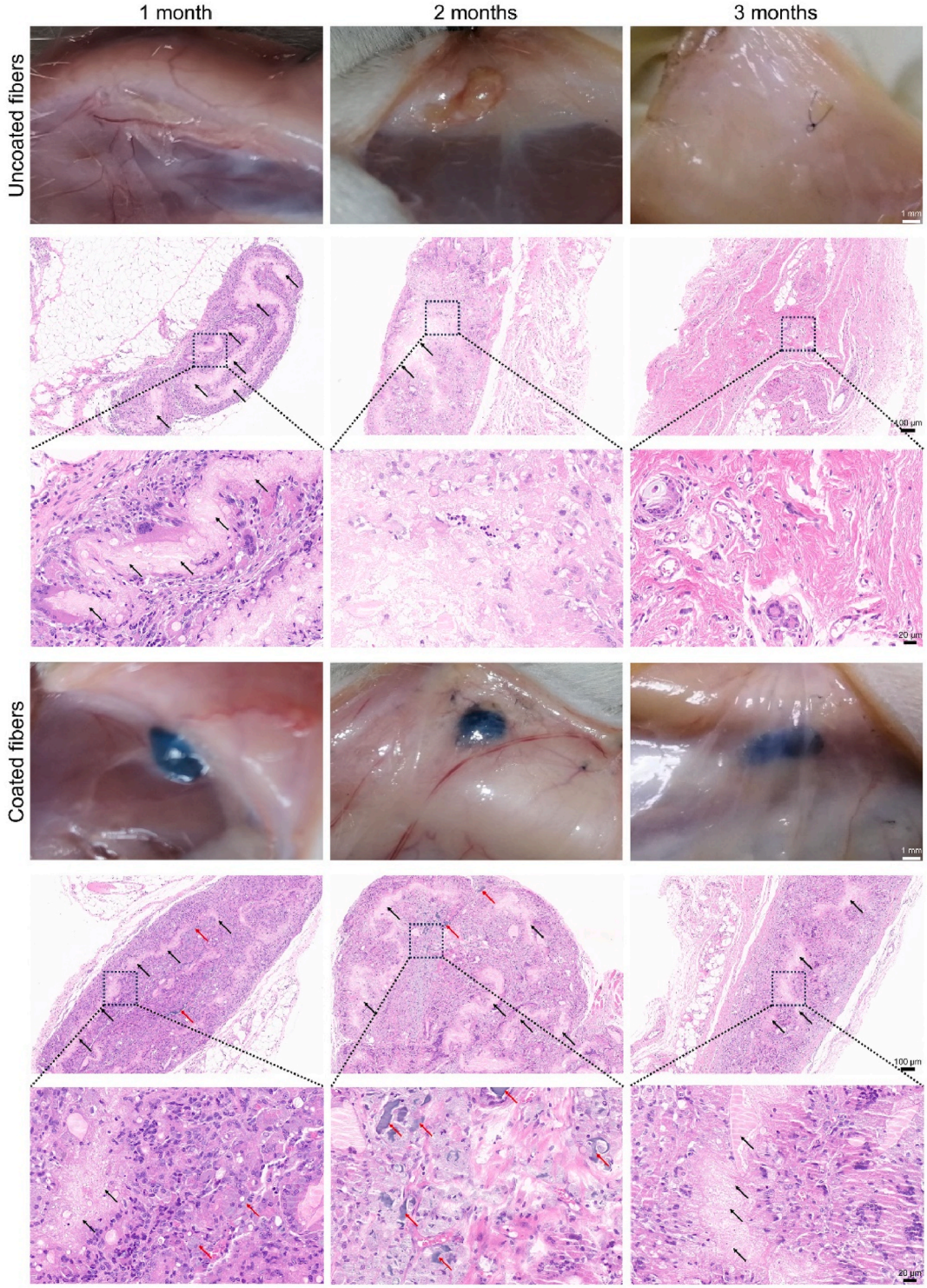

Fig. 4. The external phase of *in vivo* degradation and H&E staining were performed on PLGA fiber films at various time points. No evident edema, oozing, or inflammation was observed in the implanted area of the fiber film during the external phase evaluation. Additionally, H&E staining revealed no significant aggregation of inflammatory cells within both the PLGA fiber film and its coating area, indicating excellent biocompatibility of the implanted material. The magnified area is indicated by a black square, while PLGA fiber films are denoted by black arrows and PEDOT:PSS coating by red arrows (n = 3, n indicates the number of samples tested in each group). (For interpretation of the references to colour in this figure legend, the reader is referred to the Web version of this article.)

in cell adhesion to the surface of the fiber film, it also significantly influences cell proliferation [22]. The water contact angles of the uncoated and coated PLGA films were 123.07 ± 2.01° and 54.03 ± 3.94°, respectively ($p < 0.001$) (Fig. 3K). Consequently, the hydrophilicity of the coated film was significantly enhanced, thereby promoting cell adhesion and proliferation.

3.6. The in vitro and in vivo degradation of porous PLGA fiber films coated with PEDOT:PSS

The polymer PLGA is widely recognized for its exceptional biocompatibility, excellent biodegradability, and ease of fabrication, making it highly suitable for various applications in tissue engineering. A notable advantage of PLGA NGCs lies in their biodegradable nature, eliminating the need for a secondary surgical procedure to remove them. To ensure optimal performance, the degradation rate of NGCs must align with the pace of nerve regeneration. The optimal degradation time of PLGA allows for sufficient mechanical support for PNR without hindering its progress. After 100 days of degradation, the nonporous PLGA fiber film, porous PLGA fiber film, and coated porous PLGA fiber film degraded to 51.26 ± 0.93 %, 52.15 ± 0.76 %, and 51.24 ± 0.21 % of their original qualities, respectively (Fig. S4). Due to the UVO treatment applied to the fiber films, elastase could effectively penetrate the films. The appropriate degradation rate of PLGA fiber films creates favorable conditions for PNR.

Additionally, PLGA is among the limited number of biomaterials that have been approved by the food and drug administration (FDA) for both experimental and clinical applications [51]. Numerous previous studies have demonstrated the suitability of PLGA as a material for PNR [52–55]. Faroni et al. revealed that cylindrical NGCs composed of PLGA exhibited excellent flexibility, biodegradability, permeability, and facilitated easy suturing of transected nerve stumps. When the NGC was surgically implanted into a 12-mm gap in the rat sciatic nerve, resulting in the successful PNR [56]. Furthermore, PLGA has been extensively investigated for its ability to provide adequate mechanical support for nerve regeneration in numerous studies [25,57,58]. These findings demonstrate the reliability of using PLGA for the preparation of NGCs. In addition to its applications in PNR, PLGA has also been utilized in various other medical fields without limitations imposed by its degradation products, including skin grafting, wound closure, and micro- and nanoparticles. Various applications of PLGA drug microsphere preparation have also been reported, including the utilization of PLGA microspheres as carriers for protein and enzyme drugs, which is a prominent area of research [59]. Additionally, PLGA is employed as a drug carrier in Lupron Depot, an effective treatment for advanced prostate cancer.

We implanted uncoated and coated PLGA fiber films into the subcutaneous fascia layer of the rat dorsum for *in vivo* degradation testing (Fig. S5A). The weight changes of the rats were monitored over 3 months post-implantation. Body weight variations can reflect both rat growth and potential implant toxicity. All groups exhibited an increase in body weight following fiber film implantation, indicating no significant impact on their growth (Fig. S5B).

Fig. 4 displays the uncoated and coated PLGA fiber films at 1, 2, and, 3 months post-implantation, along with the corresponding H&E staining results. At the mark point, the uncoated PLGA fiber film was observed to be encapsulated by soft tissue, accompanied by an inflammatory infiltrate surrounding it 1 month after surgery. This phenomenon primarily resulted from the *in vivo* degradation of PLGA, which is a complex process involving various cell types such as eosinophils and macrophages [60]. After 2 months post-surgery, only a minimal amount of residual PLGA was observable, and the cellular infiltration had essentially subsided. 3 months following implantation, complete disappearance of PLGA occurred, rendering the implanted area indistinguishable from normal tissue. Regarding the coated fiber film, no conspicuous aggregation of inflammatory cells surrounding the coating was observed, thus confirming its excellent biocompatibility. The presence of undegraded coated PLGA films at the 3-month postoperative mark suggests that the conductive coating effectively impedes cell-PLGA interaction and retards *in vivo* degradation of the film. The conductive coating exhibited excellent biocompatibility as evidenced by the absence of significant cellular infiltration in its vicinity.

An appropriate degradation rate is crucial for NGC. Generally, the PNR process takes approximately 2–3 months. Therapeutic studies of NGCs for long-distance nerve defects may even extend up to 3–48 months. Commercial neural scaffolds approved by the FDA, such as Neuroflex and NeuroGen, achieve complete degradation after 8 and 48 months of implantation, respectively [61]. The fiber films were subcutaneously implanted in the dorsal region of rats, allowing the mucous membrane layer and tissue fluid to have unrestricted access to the films after suturing the incision, thereby significantly expediting their degradation. However, when the films were utilized as NGCs for bridging nerve defects, they were situated within the interstitial spaces of the rat legs' muscles, thereby minimizing direct exposure to tissue fluids and various digestive enzymes, consequently significantly retarding their degradation process. The relative structural integrity of NGCs was also evident in our postoperative specimens of nerves and muscles removed after 3 months, thus providing robust mechanical support to facilitate nerve regeneration.

The research on PEDOT has been extensive due to its superior electrical conductivity and chemical stability [16]. Park et al. concluded that PEDOT:PSS shows the most promising potential for long-term implantation in the central nervous system (CNS) [62]. The remarkable chemical stability of PEDOT in aqueous solutions at both room temperature and elevated temperatures can be attributed to the stabilizing effect of sulfur and oxygen on positive charges [63]. Due to the limited biodegradability of CPs, developing methods to incorporate biodegradability into these materials is a crucial and formidable task in fabricating tissue engineering scaffolds [64]. These approaches encompass incorporating hydrolyzable side groups into monomers and creating composites of CPs with biodegradable polymers [65,66]. In our experiments, we prepared a composite consisting of PLGA and PEDOT:PSS, which was diluted to reduce its cytotoxicity while ensuring its electrical conductivity. The non-degradable properties inherent in PEDOT:PSS did not exhibit any discernible impact on nerve regeneration, as evidenced by the results obtained from animal experiments and H&E staining.

PNR relies on the reconstruction of the local microenvironment, which encompasses critical factors such as intraneural vascularization, bioelectrical conduction, bioenergetic metabolism, and immune response [67]. Although PLGA possesses desirable mechanical properties and processability, its hydrophobicity and lack of bioactive sites restrict its application. Evidence suggests that appropriate surface modification of PLGA can facilitate the development of ideal nerve grafts that closely resemble natural nerve microstructure [68]. Further investigation is necessary to examine the impact of various PLGA scaffolds on the microenvironment of nerve regeneration. Lactic acid, a degradation product of PLGA, has been shown to enhance the expression of pro-angiogenic factors in vascular endothelial cells and activate pro-angiogenic signaling pathways, leading to significant improvements in vascular regeneration [69]. However, interactions between biomaterials and tissues as well as the effects of biomaterial degradation products on angiogenesis and nerve regeneration are complex and diverse, requiring further extensive research [70].

3.7. The impact of PLGA fiber films with a coated porous surface on cellular behavior

The SEM images revealed that SCs adhered well to the coated porous PLGA fiber films and exhibited bipolar extension, likely due to the nanoscale surface roughness of the film that mimics natural tissue structures (Fig. S6A). Electrospinning techniques can be used to prepare

fibers with different surface morphologies (porous or grooved), which effectively enhances their surface roughness [12]. A previous study has reported that changes in surface roughness within the range of large biomolecules to cell size (10 nm - 10 μm) can impact the biological effects of the interface [71]. The modification of micro-scale surface roughness could enhance the adsorption and bioactivity of various proteins, thereby promoting cell adhesion, proliferation, and extracellular matrix (ECM) synthesis [71]. The previous study has established a correlation between the biological effects of material surface roughness the hydrophilicity [72]. However, it should be noted that rough electrospinning fibers possess a larger contact area with cells compared to smooth fibers, thereby promoting cell adhesion and growth. Consequently, they are deemed more suitable for applications in tissue engineering PNR [12].

The coated aligned porous PLGA fibers exhibited not only anisotropic physical properties but also influenced the cellular behavior. As shown in Fig. S6B, PC-12 cells displayed a distinct inclination towards bipolar extension on the PLGA fibers, indicating that these fibers could regulate cell spreading morphology by mimicking the natural extracellular environment. In the absence of ES, PEDOT:PSS-coated PLGA fibers demonstrated the ability to facilitate PC-12 cell adhesion and promote directional growth. For instance, Anderson et al. reported that on PEDOT hybrid gels, PC-12 cells expressed high levels of neurogenic markers such as microtubule association protein-2 (MAP-2) and β-micro tubulin III, leading to enhanced dendritic and axonal growth [73].

We analyzed the viability of SCs and PC-12 cells in the PEDOT:PSS solution using calcein AM and PI staining (Fig. 5A). The majority of cells in each group exhibited green fluorescence, indicating their live status, while only a small proportion showed red fluorescence, suggesting cell death. The observed normal morphology of live cells indicated robust cellular activity, confirming that the PEDOT:PSS solution did not exhibit any toxicity towards nerve cells. These findings were further supported by double staining for living/dead cells and CCK-8 assay, which demonstrated that the optimal concentration of PEDOT:PSS solution had no inhibitory effect on nerve cell proliferation.

Additionally, the various morphologies of the conduit surface exert distinct influences on cell growth. Li et al. employed a microinjection molding technique to fabricate chitosan films with grooves of different sizes and observed that when the width of the grooves (10 μm) was smaller than the cell size, SCs exhibited random spreading behavior on the surface. Nevertheless, for patterns with a similar scale to the cell size (20–30 μm), the SCs exhibited directionally growth along the grooves [74]. Therefore, the fabrication of scaffolds with specific surface characteristics proved advantageous for PNR. It was hypothesized that combining morphologies and ES would synergistically enhance PNR [74]. This hypothesis will be examined in this study using the animal model.

A previous study has indicated that the macrophage phenotype may also be influenced by the cellular environment in which they are cultivated. We conducted a comparison of various electrospinning fibers to assess their impact on macrophage polarization, specifically evaluating IL-10 and TNF-α expression through ELISA analysis. TNF-α is

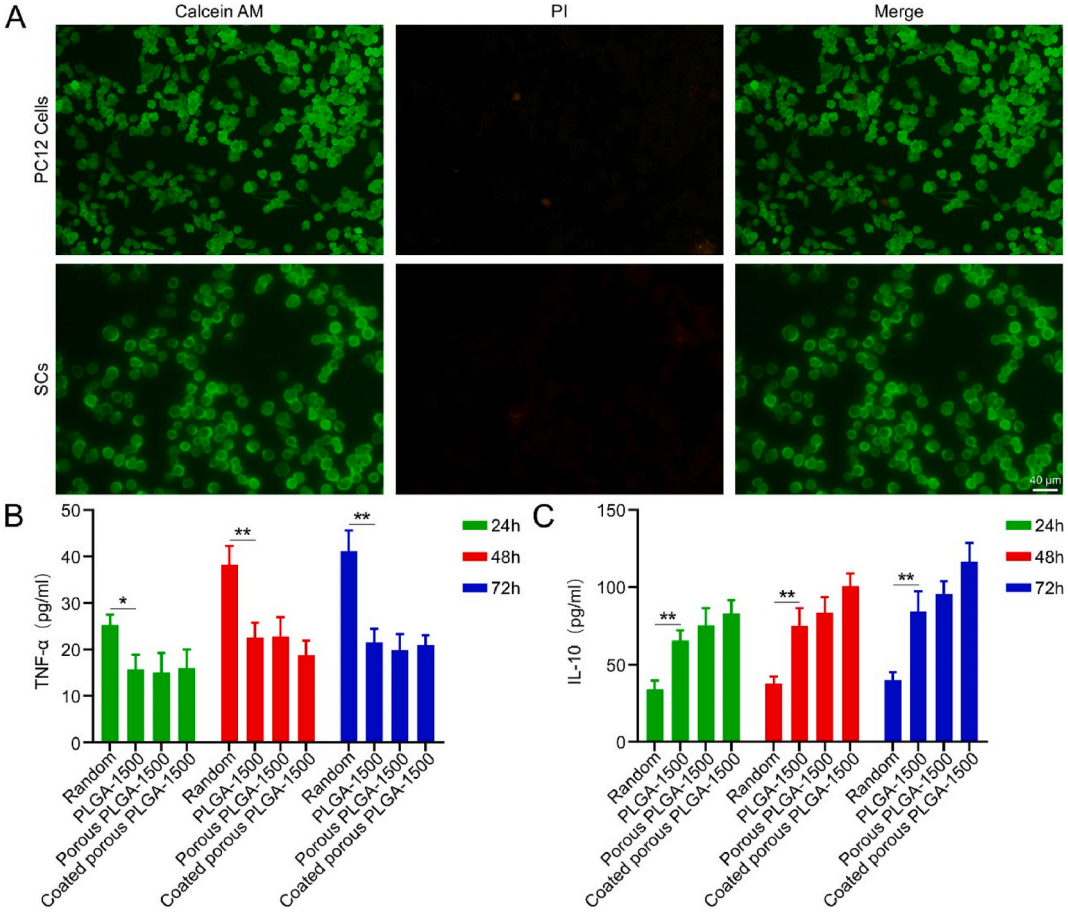

Fig. 5. The impact of electrospinning fiber alignment, surface morphology, and conductive coating on cellular response. (A) The results of double staining for living and dead cells in PEDOT:PSS solution at the optimal concentration (the left column is calcein AM staining, the middle column is PI staining, and the right column is merged photos) (n = 3, n indicates the number of experimental replicates). The secretion of TNF-α (**B**) and IL-10 (**C**) by macrophages cultured on various electrospinning fibers was quantified using the ELISA assay (n = 3, n indicates the number of experimental replicates). All statistical data are represented as mean ± SD (* indicates $P < 0.05$, ** indicates $P < 0.01$).

predominantly secreted by M1 macrophages, while IL-10 is primarily produced by M2 macrophages. The results demonstrated that macrophages cultured on aligned, porous, and coated electrospinning fibers exhibited increased secretion of IL-10 and decreased secretion of TNF-α compared to macrophages on random electrospinning fibers (Fig. 5B). However, there was no significant difference in the secretion of IL-10 and TNF-α when considering the three factors: alignment of electrospinning fibers, porous morphology of the fiber surface, and conductive coating (Fig. 5C).

3.8. Coated aligned porous PLGA NGCs for the repair of sciatic nerves in rats

The fiber film, prepared using a jetting needle consisting of a hollow steel tube with an inner diameter of approximately 1 mm, was removed from the copper foil receiver and cut into a rectangular shape measuring about 3 cm in length and 1.2 cm in width. After wrapping the fiber film around the needle 3 times and cutting it, the resulting end was sewn to the side wall using an 8-0 surgical suture to obtain the NGC.

After administering anesthetizing to the rats, the sciatic nerve was exposed and a 1-cm nerve defect model was created (Fig. 6A). Fig. 6B, C, and Fig. 6D depict the implantation of conduits in the autograft, uncoated, and coated NGC groups, respectively. The electrodes were positioned approximately 0.5 cm proximal and distal to the implanted NGC during ES treatment. The locations of the stimulating electrode, receiving electrode, and ground wire during electrophysiological testing are illustrated in Fig. 6E.

In another study, human neural progenitor cells were subjected to electrical stimulated for 12 days to study the impact of ES on these cells. It was observed that neural cells cultured on PEDOT:PSS substrates exhibited significantly enhanced axon growth compared to the control groups. The utilization of PEDOT as a substrate is advantageous due to its exceptional electrical conductivity and excellent chemical stability, while further modifications can be made to optimize the properties of this material for improved PNR. Furthermore, intracellular ion levels were found to play a pivotal role in regulating the behavior of nerve cells [75]. Wang et al. hypothesized that conductive substrates could potentially impact ion levels within nerve cells [76]. Consequently, highly conductive substrates may activate voltage-specific ion-gated channels in nerve cells, thereby eliciting diverse cellular responses [16].

The most convenient method for evaluating peripheral nerve function in the lower extremity is footprint analysis. Fig. S7A illustrates the footprints of rats from each group, taken 2 months after treatment. In the nerve defect group, PLGA-1500 group, and porous PLGA-1500 group, symptoms such as severe toe flexion contracture, extension dysfunction, abduction dysfunction of each toe, and prolonged heel-to-toe distal

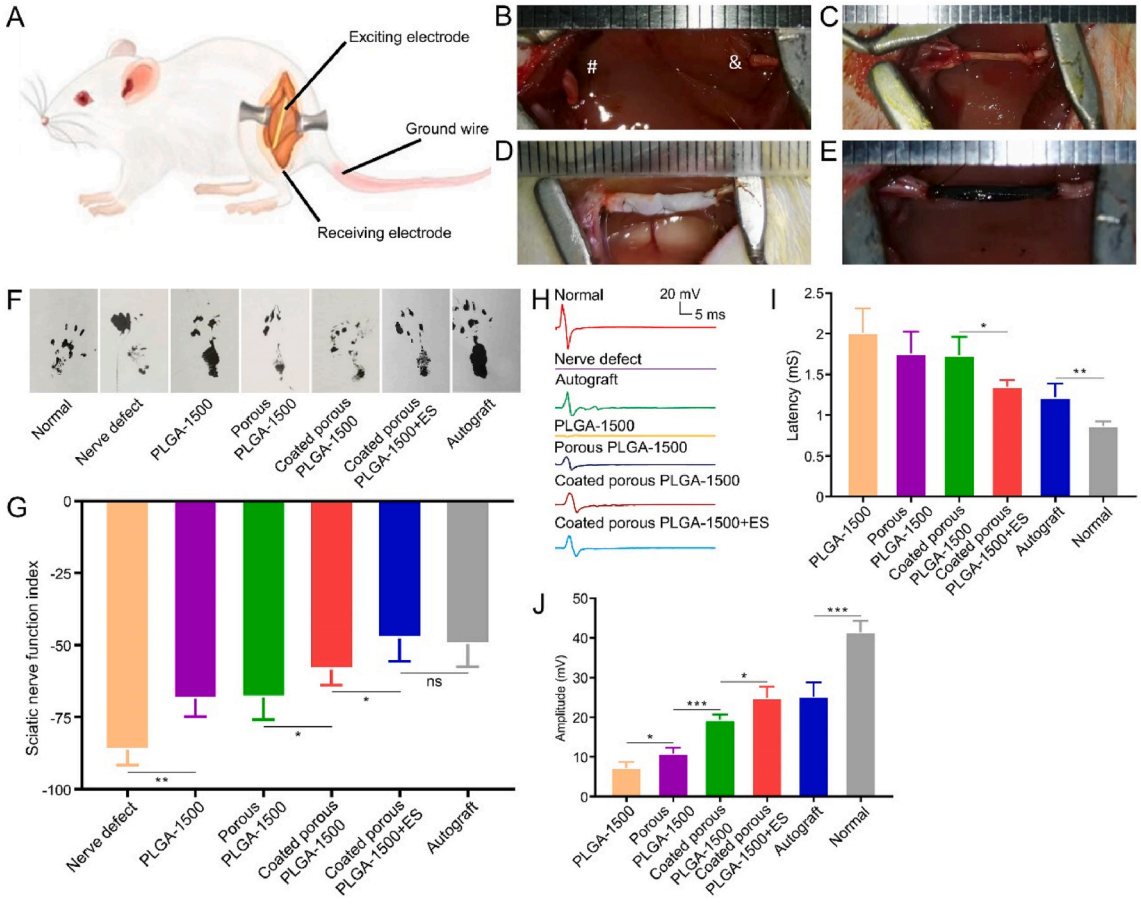

Fig. 6. Animal experimental procedures and the recovery of motor function and neurophysiology in the lower extremities of rats were evaluated after a 3-month treatment period. (**A**) Schematic diagrams illustrating the positions of ES and electrophysiological testing electrodes. (**B**) Nerve defect model, in which (&) and (#) represent the proximal and distal ends of the nerve defect, respectively (n = 10, n indicates the number of experimental animals in each group). (**C**) Autograft group (n = 10, n indicates the number of experimental animals in each group). (**D**) Uncoated NGC group (n = 10, n indicates the number of experimental animals in each group). (**E**) Coated NGC group (n = 10, n indicates the number of experimental animals in each group). (**F**) The photographs of rat footprints in each experimental group. (**G**) The SFI index of rats in each experimental group (n = 5, n indicates the number of experimental animals in each group). The neurophysiological analysis includes the waveform (**H**), latency (**I**), and amplitude (**J**) of CMAPs for each group at the 3-month detection after treatment (n = 4, n indicates the number of experimental animals in each group). All statistical data are represented as mean ± SD (* indicates $P < 0.05$, ** indicates $P < 0.01$, *** indicates $P < 0.001$).

distance indicate limited functional recovery in the lower extremity. Conversely, both coated porous PLGA-1500 + ES and autograft groups demonstrate satisfactory functional recovery.

3.9. The analysis of walking tracks

SFI served as a significant indicator of nerve function recovery in the lower extremity, with values ranging from 0 to 100, representing normal lower extremity function to complete dysfunction [77]. Compared to the groups with nerve defects, PLGA-1500 group, and porous PLGA-1500 group, rats at the coated porous PLGA-1500 + ES group exhibited improved lower extremity function ($p < 0.05$) (Fig. S7B). These findings demonstrate that after 2 months of treatment, the combination of coated aligned porous NGC and ES can effectively promote the recovery of lower extremity function.

The footprints of the rats in each group after 3 months of treatment were shown in Fig. 6F. Except for the nerve defect group, all rats exhibited improved lower extremity function compared to that at 2 months, primarily demonstrating recovery in toe abduction and toe extension function (Fig. 6G). The results of walking track analysis conducted at 3 months post-operation revealed that the alignment of electrospinning fibers, conductive coating, and ES were influential factors in promoting functional recovery of the lower extremities in rats. If sufficient recovery time was provided, these factors could potentially exhibit a synergistic effect.

3.10. Electrophysiological analysis of the sciatic nerve

Electrophysiological analysis serves as a crucial indicator for evaluating PNR. CMAPs were elicited through single ES conducted by electrodes positioned proximal to the nerve defect, and recorded by receiving electrodes located distally in the muscle. The latency and amplitude of CMAPs were identified as significant parameters (Fig. S8A). Notably, while waveforms were observed across all groups, the nerve defect group exhibited a flat horizontal line.

The latency periods of CMAPs are shown in Fig. S8B for each experimental group of rats. At 2 months post-treatment, we compared the latency between the coated porous PLGA-1500 + ES group, autograft group, and coated porous PLGA-1500 group, revealing no significant differences. This observation led us to speculate that there might be two potential causes; one being the relatively short duration of PNR, which also suggests that a 10 mm nerve defect repair in rat lower extremities may require more than 2 months. The second possibility was that the coated porous PLGA-1500 group exhibited a large variance in the results, which could also explain the lack of observed differences. The amplitude of CMAPs in each group is shown in Fig. S8C. Insufficient time for PNR resulted in no significant differences between the coated porous PLGA-1500 group, coated porous PLGA-1500 + ES group, and autograft group. The results of the PLGA-1500 group and the porous PLGA-1500 group showed a significant difference ($p < 0.05$). However, both groups exhibited reduced amplitude, indicating a weak recovery of nerve conduction function.

The CMAPs waveforms and the latency results at 3 months post-treatment are presented in Fig. 6H and I, respectively. Except for the normal group, all other groups exhibited a significant reduction in latency compared to that observed at 2 months, indicating recovery of nerve conduction function in the lower extremities. The results of the coated porous PLGA-1500 + ES group were not significantly different from those of the autograft group. However, a significant difference was observed between the results of the coated porous PLGA-1500 + ES group and the coated porous PLGA-1500 group ($p < 0.05$), suggesting that early administration of ES effectively enhances lower extremity nerve conduction function recovery.

The results of CMAPs amplitude at 3 months post-treatment are shown in Fig. 6J. The recovery of CMAPs amplitude was observed in all groups, except the normal group, when compared to that at 2 months after treatment. Notably, the coated porous PLGA-1500 + ES group exhibited the highest degree of amplitude recovery, suggesting that early application of ES during treatment effectively promotes the recovery of nerve conduction function; however, it requires sufficient time. The results of the coated porous PLGA-1500 + ES group were not significantly different from those of the autograft group at 3 months post-treatment. However, there was a significant improvement in comparison to the coated porous PLGA-1500 group ($p < 0.05$), suggesting that ES effectively promotes PNR. The amplitude of the coated porous PLGA-1500 group exhibited a significantly superior performance compared to the porous PLGA-1500 group ($p < 0.001$). Additionally, the results of the porous PLGA-1500 group also outperformed those of the PLGA-1500 group ($p < 0.05$), indicating that both the conductive coating and the porous structure independently influenced PNR and demonstrated a synergistic effect when combined.

The application of ES promotes nerve regeneration and is potentially linked to the involvement of mitochondria, which are crucial organelles in energy metabolism. ES induces a transmembrane potential across the mitochondrial membrane, thereby influencing cellular metabolism within the inner mitochondrial membrane. This process converts electrical energy into chemical bonding energy for adenosine triphosphate (ATP) synthesis and consumption, leading to an acceleration of ATP production [78]. Consequently, the released ATP may stimulate mitosis through autocrine and paracrine mechanisms, resulting in a transient increase in intracellular Ca^{2+} levels [79]. ATP-dependent P2X ligand-gated channels and morphology-sensitive stretch-activated cation channels facilitate the influx of Ca^{2+} into cells during ES [80]. Conversely, Ca^{2+} influx can impede glycolysis in the cytoplasm and aerobic respiration in the mitochondria [81]. The effects of ES on skeletal muscle cells induce the generation of reactive oxygen species (ROS) through extracellular ATP release and stimulation of P2Y1 receptors. Increased intracellular ROS levels can serve as signal transducers that potentially initiate various programs to enhance cell proliferation and differentiation [82].

3.11. Histological examination of GM

When the sciatic nerve is damaged in rats, there may be a loss of innervation in the GM and a potential shift towards protein degradation in muscle protein homeostasis. This could result in reduced muscle cell volume, weight loss, neovascularization, and increased connective tissue proliferation [83]. The GMs in all groups exhibited atrophy compared to the healthy sides (Fig. S9A). However, both the coated porous PLGA-1500 + ES group and the autograft group displayed muscle morphologies that were more similar to those of the healthy sides, with less atrophy. The Masson staining revealed that the normal GM fibrous tissue exhibited a greater myocyte size and reduced perimysial fibrous connective tissue, whereas the experimental side displayed diminished myofibril size and heightened collagen fibers.

The muscle weight percentage of the GM on the experimental sides was observed to decrease (Fig. S9B). However, due to insufficient treatment time, only the combined application of conductive coating and ES demonstrated some therapeutic effect, while either treatment method alone did not show a significant effect. In Fig. S9C, it can be seen that the diameter of GM fibers decreased in all experimental groups at 2 months after treatment. The alignment of the fibers, the porous structure of the fiber surface, and ES all contribute to promoting muscle recovery in the lower extremities. However, despite the effective promotion of muscle recovery achieved by combining ES with conductive coating, there still remains a significant difference compared to the autograft group ($p < 0.001$), which may necessitate an appropriate extension of the recovery period.

After a 3-month treatment period, the recovery of GM in each group is illustrated in Fig. 7. The GM morphology in the coated porous PLGA-1500 group, coated porous PLGA-1500 + ES group, and autograft group exhibited a closer resemblance to the contralateral morphology. Masson

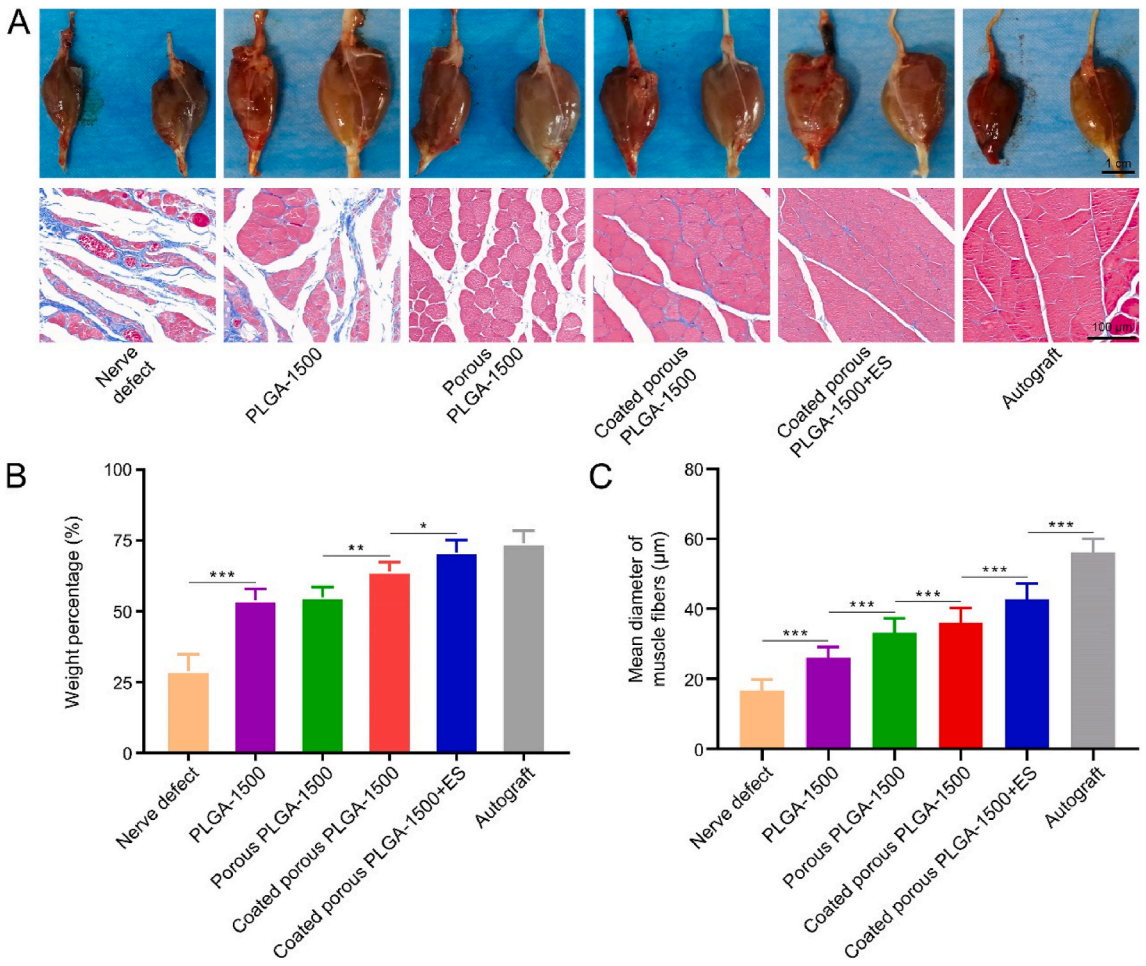

Fig. 7. Analysis of GM 3 months post-treatment. (**A**) Photographs of GM in each experimental group (left muscles were the experimental GM and right muscles were the contralateral normal GM) and Masson staining of GM. (**B**) The weight ratio of GM on the experimental side to that on the normal side (n = 5, n indicates the number of experimental animals in each group). (**C**) The mean diameter of GM fibers on the experimental side (n = 50, n indicates the number of muscle fibers in each group). All statistical data are represented as mean ± SD (* indicates $P < 0.05$, ** indicates $P < 0.01$, *** indicates $P < 0.001$).

staining revealed a reduction in the size of GM fibers within the nerve defect group, accompanied by an increase in collagen fibers surrounding the muscle due to increased, due to the loss of innervation and nerve nutrition to the target organ. In contrast, compared to these findings after 2 months of treatment, restoration of GM fibers was observed in all other experimental groups.

The degradation of NGCs was not complete 3 months post-implantation in rats (Fig. 7A). Previous studies have also demonstrated that PLGA NGCs continue to guide PNR even after 12 weeks of implantation [84]. The standard size and optimal topology of NGCs still remain a subject of controversy. Generally, conduits with thicker walls create an ideal microenvironment for promoting PNR as they offer enhanced stability for nerve growth within the conduit and prevent structural collapse [85]. However, an excessively thick wall may reduce its permeability and hinder nutrient transport into the NGC, thereby potentially impacting nerve cell proliferation [85]. For instance, increasing the scaffold's wall thickness from 200 μm to 600 μm resulted in a decrease in glucose permeability from 82 % to 53 % [85].

The experimental groups were assessed for the ratio of muscle weight on the experimental side to contralateral muscle weight (Fig. 7B) and the diameter of muscle fibers on the experimental side (Fig. 7C) after a 3-month treatment period. Notably, all groups exhibited varying degrees of recovery in GM, except for the nerve defect group, suggesting an increase in GM protein synthesis with innervation restoration. The diameter of muscle fibers decreased in the nerve defect group, which was associated with long-term denervation and reduced neurotrophic effects. The alignment of fibers, the porous structure of the fiber surface, conductive coating, and ES could enhance GM recovery, exhibiting a certain synergistic effect among them. However, when considering muscle fibers specifically, autograft remains the most therapeutically effective.

3.12. The alignment of electrospinning NGCs after implantation

The SEM images of the inner layers of NGCs implanted in rats for 3 months are presented in Fig. S10. Due to the alignment of each layer during the preparation of electrospinning fibers, subsequent layers remained aligned even after degradation. The NGC specimens extracted from rats remained intact, indicating that the alignment of NGCs could still effectively guide nerve regeneration even after 3 months of implantation. Jing et al. also reached the same conclusion in their study [84]. Furthermore, it should be noted that the alignment of electrospinning fibers also plays a crucial role in shaping the local immune environment of PNR. We have already obtained relevant conclusions from our previous cellular experiments and will further validate them in subsequent experiments.

3.13. Histological examination of regenerated sciatic nerve

To assess the regenerating nerve tissue in the different groups, histological analysis of the regenerated nerves was conducted at 2 months post-treatment using H&E staining and TEM (Fig. S11). The results

obtained from H&E staining demonstrated well-aligned normal nerve tissues. The alignment of the regenerated nerve tissue in both the coated porous PLGA-1500 + ES group and autograft group was inferior to that of normal nerves but superior to other experimental groups. The regenerated nerve tissue in the nerve defect group exhibited a loose and non-aligned structure at 2 months post-treatment, accompanied by an increased presence of vacuoles within the nerve tissue. Furthermore, local inflammation served as a crucial indicator for evaluating the efficacy of NGC in promoting PNR. Inflammatory cell infiltration, cellular edema, or fatty degeneration, indicating that the NGCs did not induce significant local inflammation. Additionally, neovascularization was observed in all experimental groups except the nerve defect group, indicating that microcirculation could create a favorable microenvironment for PNR by supplying oxygen, nutrition, and various factors [86].

TEM images were utilized to assess the regeneration of nerve axons and myelin. Low-magnification TEM images revealed the number of regenerated nerve fibers, myelination in nerve axons, reconstruction of microcirculation, and connective tissue between nerve axons. High-magnification TEM images allowed for the measurement of the diameter of the myelinated axon and the thickness of the myelin sheath. The myelin sheath provides support for the nerve axon and serves as an insulating barrier against perineural tissue, preventing mutual interference of neuroelectric signals. Moreover, myelin sheaths facilitate the conduction of action potentials between nodes of Ranvier, thereby accelerating the transmission of neuroelectric signals.

Additionally, damaged myelin sheaths play a guiding role in axon regeneration. Consequently, the thickness of regenerated myelin sheaths can serve as an indicator of nerve functional recovery. The regeneration of nerve axons and myelin sheaths can be promoted by various factors, with conductive coatings and ES having the most significant impact (Fig. S12). Although a certain therapeutic effect was observed 2 months after the implantation surgery, there still remained a notable disparity when compared to the autograft group, indicating that adequate time is also required for axonal and myelin sheath regeneration.

The regeneration of nerve tissue was evaluated at 3 months post-treatment using H&E staining and TEM (Fig. 8A). Compared to the previous assessment at 2 months, all groups exhibited significantly improved alignment of the regenerated nerve tissue, accompanied by a reduction in the number of tissue vacuoles. Furthermore, no significant local inflammation or compromised microcirculation reconstruction was observed across all groups. The morphology of the regenerated nerve tissue in the coated porous PLGA-1500 + ES group and the autograft group exhibited similarities to that of normal tissue. The number of regenerated nerve fibers was observed to increase on TEM images at 3 months post-treatment, indicating an enhancement in axon myelination and microcirculation reconstruction.

The diameter of myelinated axons and the thickness of myelin sheaths were measured in each group 3 months after treatment using high-magnification TEM images (Fig. 8B and C). Various therapeutic factors exhibited positive effects on the regeneration of myelinated nerve axons and myelin sheath regeneration, with ES showing the most prominent effect. The coated porous PLGA-1500 + ES group and the autograft group exhibited acceptable myelin sheath thickness at 3 months of treatment, indicating the efficacy of ES in promoting nerve axon regeneration and myelination. Furthermore, the combination of conductive NGC and ES not only enhances PNR but also facilitates the differentiation and synaptic growth of primary neurons. Physical and chemical signals at the material interface facilitate the recognition and transmission of interactions between cells and CPs, while ES can modify cell behavior by altering the cell membrane. However, further exploration is needed to understand the mechanisms underlying cellular sensing of electrical signals [87].

3.14. Immunofluorescence analysis of regenerated sciatic nerve

We conducted immunofluorescence testing to examine the expression of various neural proteins during PNR. GFAP was found to be expressed in both the CNS and PNS, predominantly localized in astrocytes within the CNS. It plays a crucial role in maintaining cytoskeletal integrity and strength. The increased content of GFAP following PNI promotes axonal growth along topographical cues provided by fibrous scar tissues. MBP, primarily distributed in myelin sheaths and nuclei, serves as an indicator for assessing myelin sheath regeneration during PNR [88]. In addition to GFAP and MBP, we also conducted immunofluorescence staining for NF200 and Tuj-1. NF200 can be utilized to evaluate the regeneration of neurofilaments during PNR. Neurofilaments, microfilaments, and microtubules collectively constitute the cytoskeleton of neurons, providing structural support for axons and regulating their diameters. Tuj-1 serves as a distinctive protein in synaptic regeneration following PNI and can also differentiate neurons from glial cells [89].

The neural expression of SCs and axons was further assessed through GFAP and Tuj-1 triple staining (Fig. 9A). Additionally, the regeneration efficiency of neurofilaments and myelinated fibers was evaluated using NF200 and MBP triple staining, respectively (Fig. 9B). A semi-quantitative analysis of fluorescence density was also utilized to assess the expression of specific proteins related to PNS, including GFAP, Tuj-1, NF200, and MBP (Fig. 9C). The findings indicated that the combination of ES with implanted NGCs exhibited superior promotion of axonal regeneration and myelination compared to other experimental groups.

3.15. Immunocyte analysis of regenerated sciatic nerve

The accumulation of macrophages in injured and regenerated nerves is abundant. Cells isolated from the sciatic nerve were examined. Cells expressing CD11b and CD86 were classified as M1 macrophages, while cells expressing CD11b and CD206 were categorized as M2 macrophages. CD86 provides the necessary costimulatory signals for T-cell activation and is widely recognized as a cell surface marker indicative of M1 macrophages. Conversely, CD206, a mannose receptor associated with endocytosis, serves as a specific marker for M2 macrophage [90]. These distinct subsets of macrophages coexist within injured and regenerated sciatic nerves and can be distinguished by different quadrants (Fig. S13A).

The macrophages can be categorized into two distinct phenotypes: the M1 pro-inflammatory phenotype, which is classically activated, and the M2 anti-inflammatory phenotype, which is alternatively activated. Upon polarization, these macrophages exhibit differential expression of various cellular markers such as receptors, enzymes, trophic factors, chemokines, and cytokines [91]. Typically, M1 macrophages are considered to have neurotoxic properties while M2 macrophages play a role in promoting axonal regeneration [92].

In our study, the nerve defect group exhibited the highest percentage of M1 macrophages, which was significantly different from all other experimental groups. However, ES was able to decrease the proportion of M1 macrophages. Nevertheless, ES alone did not have a significant effect on M2 macrophages and only induced an increase in their proportion when combined with conductive coatings and porous morphology (Fig. S13B). This observation may be attributed to the influence of these factors on macrophage behaviors mediated by macrophage stimulating factor (M-CSF) [93]. The expression of CSF-1R in tissue macrophages and monocytes facilitates the migration of monocytes into injured nerves and influences the differentiation and survival of tissue macrophages [94]. Conversely, M-CSF stimulation has a diminished effect on M2 macrophages, suggesting that a combination of factors may be necessary to modulate M2 macrophage polarization [95]. Previous studies have previously reported that M2 macrophages secrete IL-10 [96]. However, our findings demonstrate that the porous morphology and conductive coatings do not exert a significant impact

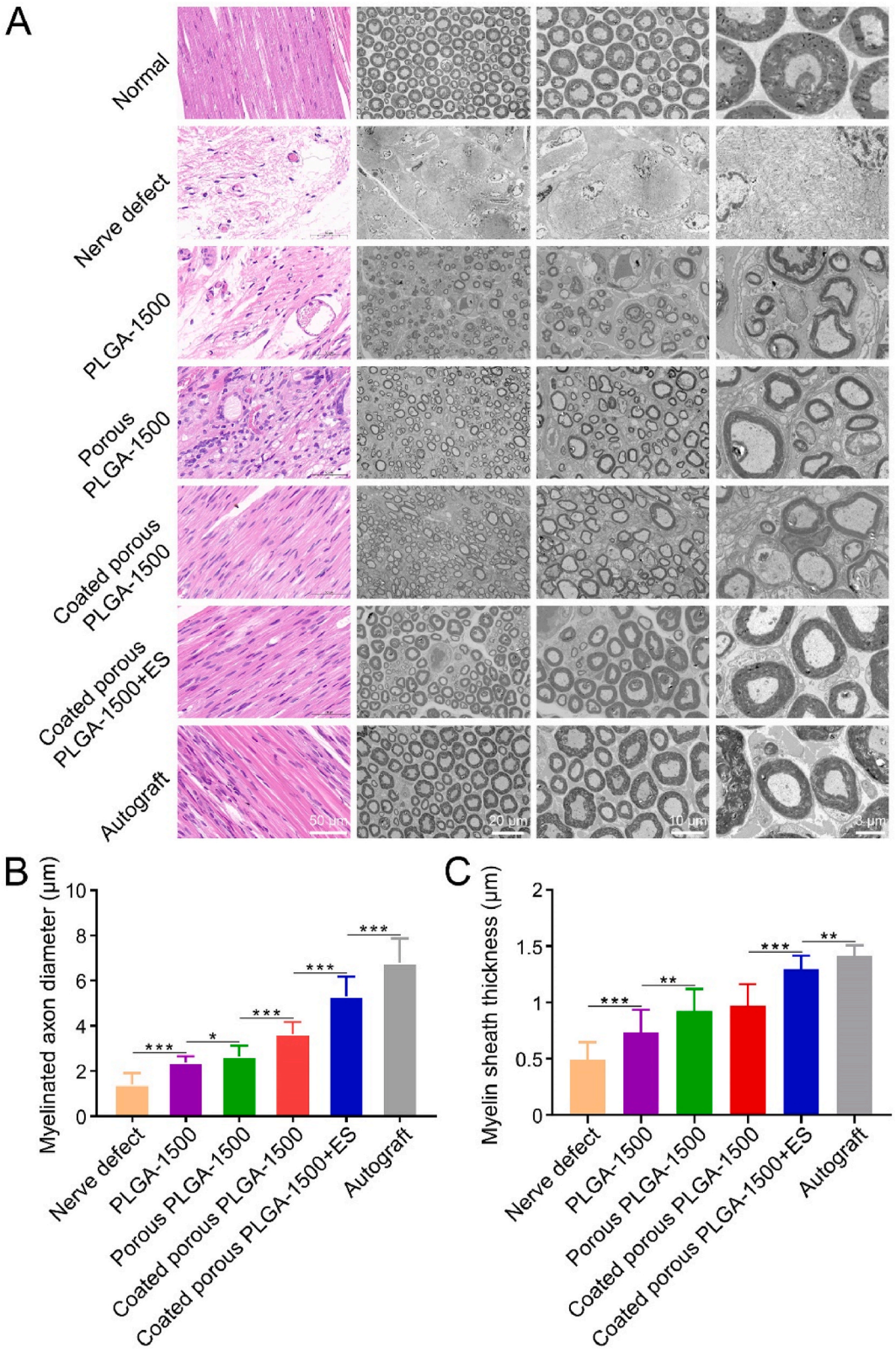

Fig. 8. Histologic examination of regenerated nerves at the 3-month post-treatment time point. (**A**) The regenerated nerves in each group were evaluated at 3 months after treatment using H&E staining and TEM images (n = 5, n indicates the number of samples tested in each group). (**B**) The diameter of myelinated axons (n = 20, n indicates the number of myelinated axons in each group) and (**C**) the thickness of myelin sheath (n = 20, n indicates the number of myelin sheaths in each group) in each group at 3 months after treatment. All statistical data are represented as mean ± SD (* indicates $P < 0.05$, ** indicates $P < 0.01$, *** indicates $P < 0.001$).

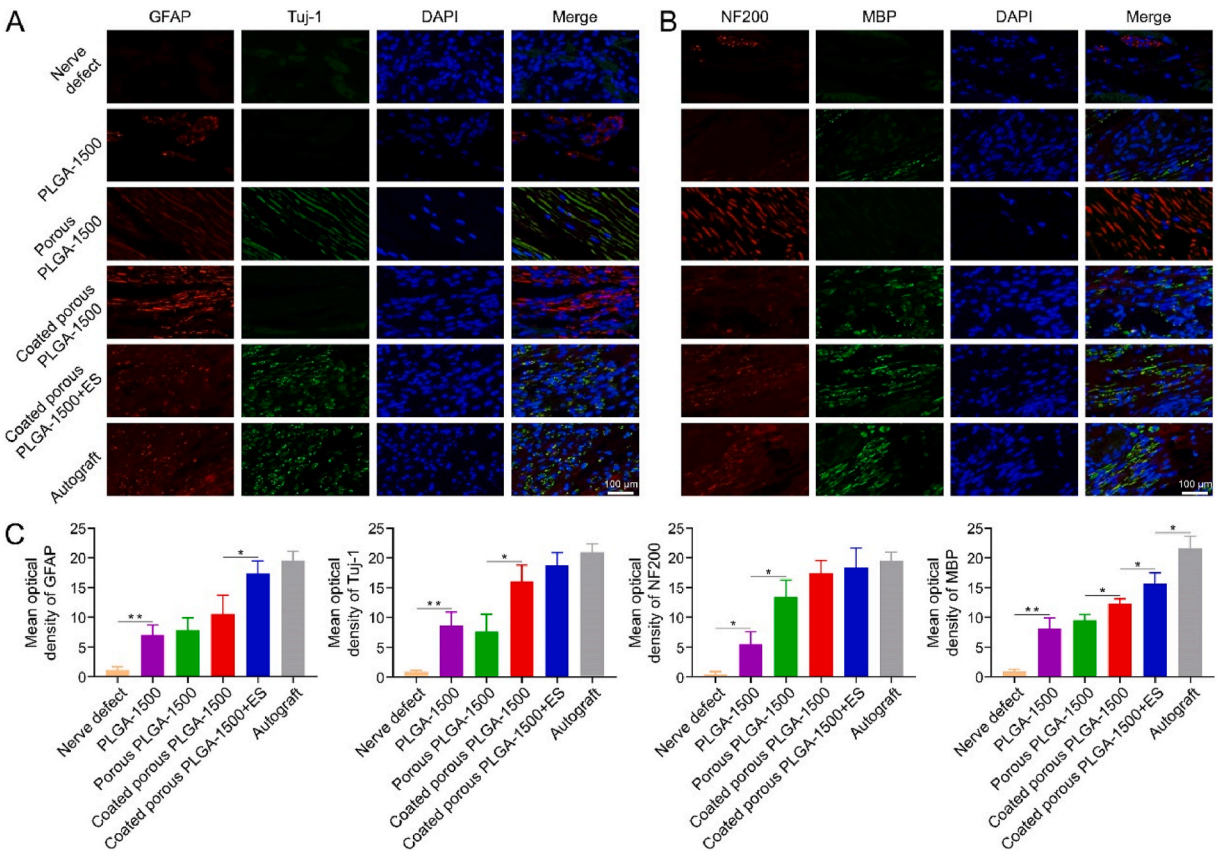

Fig. 9. Immunofluorescence analysis was performed on regenerated sciatic nerves 3 months post-treatment. (**A**) The triple immunofluorescent staining of GFAP and Tuj-1 (red, GFAP; green, Tuj-1). (**B**) The triple immunofluorescent staining of NF200 and MBP (red, NF200; green, MBP). (**C**) The fluorescence density of GFAP, Tuj-1, NF200, and MBP was quantified using a semiquantitative approach (n = 3, n indicates the number of samples tested in each group). All statistical data are represented as mean ± SD (* indicates $P < 0.05$, ** indicates $P < 0.01$). (For interpretation of the references to colour in this figure legend, the reader is referred to the Web version of this article.)

on IL-10 secretion (Fig. 5C). Consequently, we postulate that disparities in local immune cell populations may constitute one of the mechanisms through which ES facilitates PNR.

3.16. MEP staining of GM

The MEP staining of the GM at 3 months post-surgery is presented in Fig. S14. Significant variations in MEP levels were observed among all experimental groups, except for the nerve defect group. The quantification of MEPs within individual low-magnification visual fields across different experimental groups (Fig. S15). Except for the porous structure of the fiber surface, all other factors contribute to the enhancement of MEPs recovery. The results from the coated porous PLGA-1500 + ES group were no longer significantly different from those of the autograft group, indicating that ES also plays a crucial role in promoting neurosecretory function recovery.

3.17. Transcriptomic analysis of regenerated sciatic nerve

We summarized the results of transcriptomic testing on animal specimens, focusing on data quality. RNA integrity was assessed using the RNA nano 6000 assay kit of the Bioanalyzer 2100 system (Agilent Technologies, CA, USA). Following raw data filtering, sequencing error rate and GC content distribution were checked to obtain clean reads and data for subsequent analysis. These findings are presented in Table 2. The NGC group refers to the coated porous PLGA-1500 group, while the ES-NGC group represents the coated porous PLGA-1500 + ES group. The number of raw bases should exceed 6G to avoid false-negative results, and the data volume in each of our samples meets the testing criteria. The percentage of bases in the Q20 index (error rate less than 1 %) exceeds 96 % for all samples, while the percentage of bases in the Q30 index (error rate less than 0.1 %) is above 91 %, thus confirming the validity of our sequencing data.

Table 2
Summary of sample sequencing data quality.

Sample	Raw-bases	Clean-reads	Clean-bases	Error-rate	Q20	Q30	GC-pct
NGC-1	6.94G	44317574	6.65G	0.01	97.61	93.49	48.86
NGC-2	7.04G	44747210	6.71G	0.01	97.44	92.92	49.79
NGC-3	7.15G	43373290	6.51G	0.01	98.31	95.17	48.81
ES-NGC-1	7.18G	45322872	6.8G	0.01	97.82	93.94	49.48
ES-NGC-2	7.37G	47251238	7.09G	0.01	97.6	93.41	50.31
ES-NGC-3	8.33G	53080184	7.96G	0.01	97.69	93.58	50.33
Autograft-1	7.28G	46442988	6.97G	0.01	97.55	93.21	49.67
Autograft-2	7.82G	50945006	7.64G	0.01	99.35	97.98	53.83
Autograft-3	7.22G	45847408	6.88G	0.01	97.8	93.82	49.4

The transcriptomics results were subjected to statistical analysis to identify gene differences. As shown in the volcano plot, there were 807 up-regulated and 1315 down-regulated DEGs observed between the coated porous PLGA-1500+ES group and the coated porous PLGA-1500 group. The higher number of DEGs between these two groups suggests that the process and mechanism involved in rat sciatic nerve repair exhibit greater disparity.

The GO enrichment analysis revealed that the DEGs between the two groups were primarily associated with behaviors such as cation transmembrane transporter protein activity, actin filament-based processes, vascular development, chemical synaptic transmission, and paracrine transsynaptic signaling. The repair processes of ES-related nerves involve several crucial signaling pathways, including the transmembrane receptor protein tyrosine kinase signaling pathway and

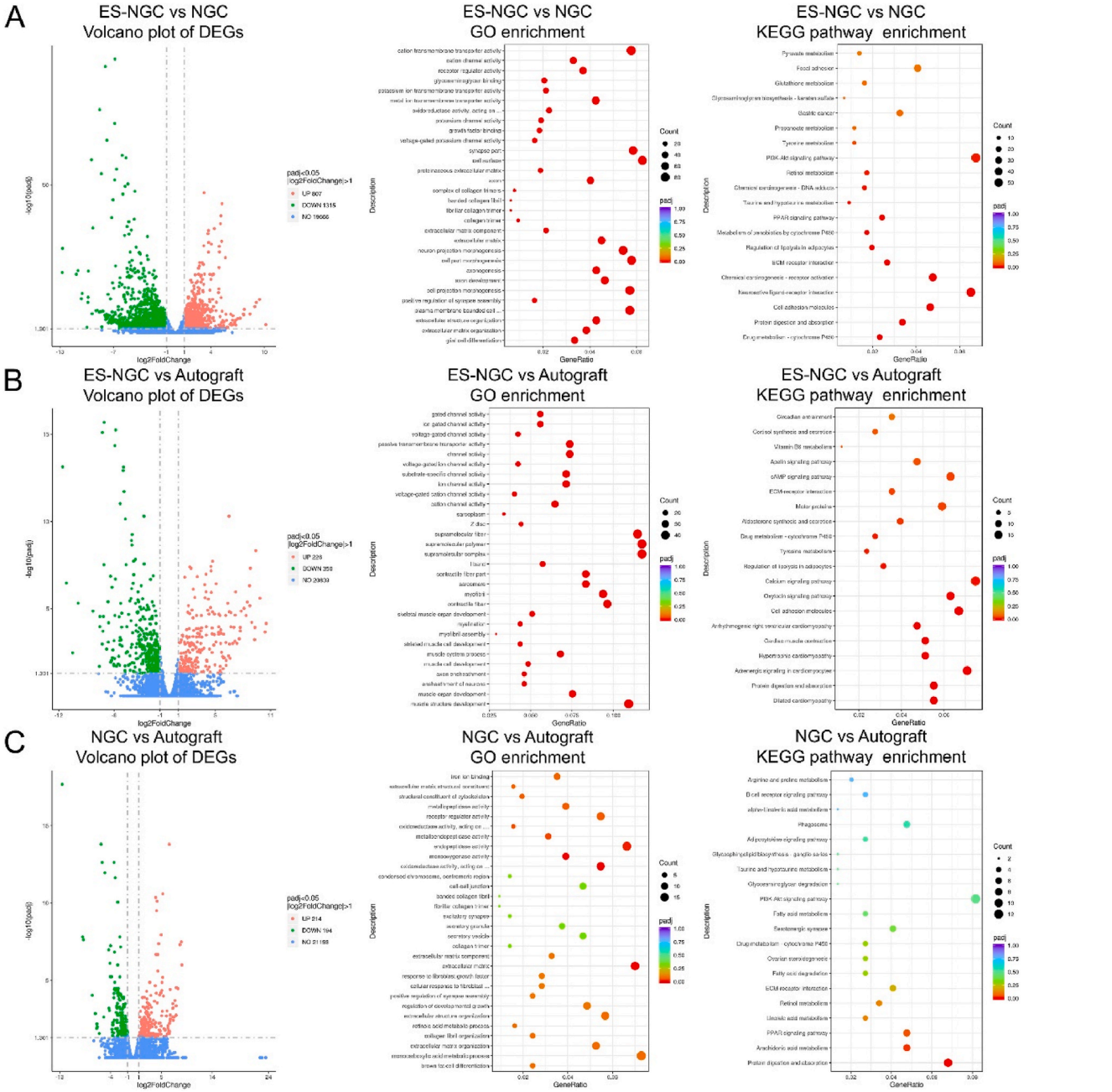

Fig. 10. Transcriptomic profiles of regenerated sciatic nerves. (**A**) A volcano plot illustrating the DEGs between the coated porous PLGA-1500 + ES group and the coated porous PLGA-1500 group is presented. The significantly up-regulated DEGs are represented by red dots, while the down-regulated DEGs are indicated by green dots. Furthermore, GO enrichment analysis and KEGG pathway enrichment analysis were conducted to compare the differences between the coated porous PLGA-1500 + ES and coated porous PLGA-1500 groups (n = 3, n indicates the number of samples tested in each group). (**B**) A volcano plot was generated to compare the DEGs between the coated porous PLGA-1500 + ES group and the autograph group. The significantly up-regulated DEGs are represented by red dots, while the down-regulated DEGs are indicated by green dots. Additionally, GO enrichment analysis and KEGG pathway enrichment analysis were performed to explore the functional annotations and pathways associated with these two groups (n = 3, n indicates the number of samples tested in each group). (**C**) A volcano plot was generated to compare the DEGs between the coated porous PLGA-1500 group and the autograph group. The significantly up-regulated DEGs are represented by red dots, while the down-regulated DEGs are indicated by green dots. Additionally, GO enrichment analysis and KEGG pathway enrichment analysis were performed to explore the functional annotations and pathways associated with these two groups (n = 3, n indicates the number of samples tested in each group). (For interpretation of the references to colour in this figure legend, the reader is referred to the Web version of this article.)

mitogen-activated protein kinase (MAPK) cascade. These pathways play vital roles in cellular signaling reception and transmission, as regulation of cellular gene expression (Fig. 10A) [97].

The volcano plot revealed the presence of 226 up-regulated and 350 down-regulated DEGs between the coated porous PLGA-1500 + ES group and the autograft group. Through integration of GO and KEGG pathway analyses, it was determined that ES primarily facilitated nerve function restoration by regulating cytoskeleton formation, transmembrane transport of substances, as well as promoting chemical signaling at synapses to achieve reestablishment of nerve innervation and trophic function in the target organ.

Through these pathways, the combination of ES and NGC effectively facilitated nerve function restoration, rendering it the experimental group with a repair effect most comparable to that of the autograft group (Fig. 10B). The volcano plot revealed the presence of 214 up-regulated and 194 down-regulated DEGs between the coated porous PLGA-1500 group and the autograft group. GO and KEGG pathway analysis demonstrated that the coated porous aligned NGCs exhibited superior regulation of various enzyme activities, including oxidoreductase, monooxygenase, and endopeptidases (Fig. 10C). The enzymes played crucial roles in redox reactions, substance metabolism, and muscle recovery promotion. As a result, the coated porous PLGA-1500 group exhibited partial restoration of lower limb nerve function in rats. When NGC was implanted in combination with ES, the synergistic effect of multiple treatment modalities effectively facilitated the recovery of lower extremity function in rats.

3.18. The evaluation of nutritional status and organ toxicity in rats

The body weight changes of the rats in each group 3 months after treatment, and no significant difference was observed among the groups (Fig. S16). This suggests that the rats were well-nourished and properly raised with unrestricted access to food and water, as well as minimal interference between cage mates. Although lower limb function was impaired following nerve dissection, resulting in foot phagocytosis, these factors did not affect their ability to obtain water and food; hence their body weight tended to increase. The frequent administration of anesthesia and ES during the initial period following NGC implantation may potentially impact the growth status of the rats. However, the body weight trend observed within the first 10 days post-surgery indicates that anesthesia and ES have minimal effect on the physiological status of rats, as their body weight continues to exhibit an upward trajectory. The consistent increase in body weight among rats also signifies that nerve repair processes are being conducted under favorable physiological conditions.

The histopathological analysis of the heart, liver, spleen, lung, and kidney from both the coated porous PLGA-1500 + ES group and autograph group demonstrated consistent tissue morphology and structure throughout the entire implantation period (Fig. S17). Overall, these findings indicate that the treatment and degradation process of the NGC did not induce an inflammatory response or exhibit any toxicity to the rats during the entirety of the treatment period.

4. The limitations of the current research and directions for future studies

The present research studied the impact of organic solvents on the fabrication of porous electrospinning fibers, which were also strongly influenced by ambient humidity. Xuan et al. reported an increase in the presence of elliptical pores on the fiber surface with rising humidity levels and observed that pore diameter was larger under higher humidity conditions compared to lower humidity levels [98]. Although there were no statistically significant differences in pore sizes at the two humidity levels, it implies that various factors, such as collector temperature, humidity level, solvent used for preparation, and applied voltage, may influence nanopore formation. These factors should be systematically explored in future studies.

Our study demonstrated that exogenous ES can promote PNR. However, previous studies have presented conflicting findings regarding the effects of ES on nerve cell behavior. For instance, Sun et al. reported that ES accelerated the proliferation of SCs on PPy coatings [99]. However, Koppes et al. showed that ES did not exert a significant influence on SC growth [100]. Although our results were well validated by multiple experiments, future studies could be conducted using more optimized experiments. In future studies, efforts can be made to incorporate relevant bioactive molecules or other surface topologies onto the inner surface of NGCs to achieve enhanced nerve repair outcomes or address nerve defects across longer distances.

Future studies should also explore the mechanisms underlying neural stem cell differentiation in response to ES and assess the role of diverse neuronal populations in PNR, as well as elucidate the interplay between cells and implanted scaffolds. Unanswered questions include whether exogenous cells effectively promote nerve regeneration and the specific mechanisms by which these cells facilitate this process. Further studies are required to explore the potential clinical applications of NGCs combined with ES in the future. Additionally, efforts should be made to enhance the biodegradability and compatibility of conductive coatings, while simultaneously reducing their toxicity without compromising their conductivity.

Previous studies have demonstrated that the presence of regenerating vessels in the conduit does not directly correlate with the recovery of nerve function [68]. Therefore, it is crucial to investigate whether regenerative vessels play distinct roles at different stages of PNR. Additionally, exploring whether a higher number of vessels leads to more effective nerve regeneration is essential for a comprehensive and in-depth understanding of vascular factors within the microenvironment of PNR. However, further investigation is required to determine whether the acidic microenvironment significantly affects the differentiation and maturation of SCs. Additionally, it is worth exploring whether acidification of the regenerative microenvironment has a significant impact on PNR through its effects on macrophages or fibroblasts. Our studies, as well as previous related research, have established a robust theoretical foundation for the promotion of PNR by PLGA NGCs. Furthermore, these studies have provided compelling and lucid evidence regarding the properties of PLGA NGCs and their application in PNR. In an ideal regeneration environment, biomaterials should strike a delicate balance between positive and negative effects.

Many studies have employed ES for nerve regeneration. However, ES also possesses certain limitations. Firstly, the current does not specifically target cells and tissues, potentially affecting non-target ones as well. Additionally, there exists a resistance between the electrode and the target organ, leading to attenuation of current strength. Moreover, although ES promotes cell proliferation, it may result in the disorganized proliferation of cells [74]. However, the intricate nature of surgical procedures and the inherent uncertainty associated with ES elevate the surgical risk, rendering the amalgamation of NGCs with exogenous ES incapable of addressing such challenges. The advancement in piezoelectric materials and utilization of implantable nanogenerators have once again underscored the immense potential of ES in biological applications [101]. These innovative ES devices have demonstrated a remarkable ability to significantly enhance PNR and are poised to become a focal point for future research.

Our understanding of PLGA and other similar biomaterials is still in its nascent stage, with numerous fundamental questions yet to be answered. Depending on the specific characteristics of the regenerated tissues and organs, a synergistic combination of polymers and biomaterials may offer the optimal solution. The NGCs prepared with further optimized polymers exhibit enhanced biocompatibility, improved plasticity, superior mechanical properties, and reduced production of acidic degradation products. By utilizing these optimized polymers to fabricate NGCs with special surface morphology, in combination with degradable and non-toxic conductive coatings and ES, we

can effectively address nerve defects exceeding 30 mm.

5. Conclusion

In this study, we utilized PLGA to fabricate porous aligned fiber films, which were coated with PEDOT:PSS polymer to prepare NGCs and combined with ES for the treatment of peripheral nerve defects in rats. The coated fiber films exhibited excellent electrical conductivity, surface topography, mechanical properties, hydrophilicity, and degradability. Moreover, they demonstrated significant biocompatibility by effectively promoting the growth of SCs and PC-12 cells without inducing cytotoxicity. Animal experiments further confirmed that the NGCs combined with ES could significantly enhance lower extremity function recovery and improve the therapeutic efficacy of nerve regeneration in rats.

Funding sources

This work was supported by the National Key Research and development Program of China (2022YFC2405805), National Natural Science Foundation of China (NSFC) U23A20490, Jilin Province Science and Technology Development Plan Project (YDZJ202301ZYTS006), Doctor of excellence program (DEP), The First Hospital of Jilin University (JDYY-DEP-2023027).

CRediT authorship contribution statement

Kai Liu: Writing – original draft, Visualization, Validation, Software, Methodology, Investigation. **Shuai Yan:** Validation, Software, Methodology, Investigation, Conceptualization. **Yao Liu:** Visualization, Software, Methodology, Investigation. **Jianfeng Liu:** Visualization, Software, Investigation. **Ruijun Li:** Writing – review & editing, Visualization, Validation, Supervision, Resources, Project administration, Funding acquisition. **Lirong Zhao:** Writing – review & editing, Visualization, Validation, Supervision, Resources, Project administration, Funding acquisition. **Bin Liu:** Writing – review & editing, Visualization, Validation, Supervision, Resources, Project administration, Funding acquisition.

Declaration of competing interest

The authors declare that they have no known competing financial interests or personal relationships that could have appeared to influence the work reported in this paper.

Data availability

Data will be made available on request.

Appendix A. Supplementary data

Supplementary data to this article can be found online at https://doi.org/10.1016/j.mtbio.2024.101064.

References

[1] Y. Yang, C. Rao, T. Yin, S. Wang, H. Shi, X. Yan, et al., Application and underlying mechanism of acupuncture for the nerve repair after peripheral nerve injury: remodeling of nerve system, Front. Cell. Neurosci. 17 (2023) 1253438, https://doi.org/10.3389/fncel.2023.1253438.

[2] E. Contreras, S. Traserra, S. Bolívar, N. Nieto-Nicolau, J. Jaramillo, J. Forés, et al., Decellularized graft for repairing severe peripheral nerve injuries in Sheep, Neurosurgery 93 (6) (2023) 1296–1304, https://doi.org/10.1227/neu.0000000000002572.

[3] H.R. Shah, J.A. Bertelli, Long-term donor-site morbidity following entire sural nerve harvest for grafting, The Journal of hand surgery 48 (11) (2023), https://doi.org/10.1016/j.jhsa.2023.03.009, 1173.e1-.e7.

[4] G.N. Panagopoulos, P.D. Megaloikonomos, A.F. Mavrogenis, The present and future for peripheral nerve regeneration, Orthopedics 40 (1) (2017) e141–e156, https://doi.org/10.3928/01477447-20161019-01.

[5] V.O. Castro, C. Merlini, Aligned electrospun nerve conduits with electrical activity as a strategy for peripheral nerve regeneration, Artif. Organs 45 (8) (2021) 813–818, https://doi.org/10.1111/aor.13942.

[6] A. Joshi, S. Choudhury, S. Asthana, S. Homer-Vanniasinkam, U. Nambiar, K. Chatterjee, Emerging 4D fabrication of next-generation nerve guiding conduits: a critical perspective, Biomater. Sci. (2023), https://doi.org/10.1039/d3bm01299a.

[7] F. Mankavi, R. Ibrahim, H. Wang, Advances in biomimetic nerve guidance conduits for peripheral nerve regeneration, Nanomaterials 13 (18) (2023), https://doi.org/10.3390/nano13182528.

[8] K. Liu, L. Yan, R. Li, Z. Song, J. Ding, B. Liu, et al., 3D printed personalized nerve guide conduits for precision repair of peripheral nerve defects, Adv. Sci. (2022) e2103875, https://doi.org/10.1002/advs.202103875.

[9] S. Ghasemi, J.B. Raoof, M. Ghani, R. Ojani, Bacteria-templated ZIF-8 embedded in polyacrylonitrile nanofibers as a novel sorbent for thin film microextraction of benzoylurea insecticides, Talanta 269 (2023) 125403, https://doi.org/10.1016/j.talanta.2023.125403.

[10] H. Chen, X. Huang, M. Zhang, F. Damanik, M.B. Baker, A. Leferink, et al., Tailoring surface nanoroughness of electrospun scaffolds for skeletal tissue engineering, Acta Biomater. 59 (2017) 82–93, https://doi.org/10.1016/j.actbio.2017.07.003.

[11] C.D. Johnson, A.R. D'Amato, D.L. Puhl, D.M. Wich, A. Vesperman, R.J. Gilbert, Electrospun fiber surface nanotopography influences astrocyte-mediated neurite outgrowth, Biomedical materials (Bristol, England) 13 (5) (2018) 054101, https://doi.org/10.1088/1748-605X/aac4de.

[12] F. Zamani, M. Amani-Tehran, M. Latifi, M.A. Shokrgozar, The influence of surface nanoroughness of electrospun PLGA nanofibrous scaffold on nerve cell adhesion and proliferation, J. Mater. Sci. Mater. Med. 24 (6) (2013) 1551–1560, https://doi.org/10.1007/s10856-013-4905-6.

[13] A. Filimon, N. Olaru, F. Doroftei, A. Coroaba, S. Dunca, Processing of quaternized polysulfones solutions as tool in design of electrospun nanofibers: microstructural characteristics and antimicrobial activity, J. Mol. Liq. 330 (2021), https://doi.org/10.1016/j.molliq.2021.115664.

[14] J. Zhang, X. Zhang, C. Wang, F. Li, Z. Qiao, L. Zeng, et al., Conductive composite fiber with optimized alignment guides neural regeneration under electrical stimulation, Adv. Healthcare Mater. 10 (3) (2021) e2000604, https://doi.org/10.1002/adhm.202000604.

[15] G.B. Tseghai, D.A. Mengistie, B. Malengier, K.A. Fante, L. Van Langenhove, PEDOT:PSS-Based conductive textiles and their applications, Sensors 20 (7) (2020), https://doi.org/10.3390/s20071881.

[16] A. Magaz, B.F. Spencer, J.G. Hardy, X. Li, J.E. Gough, J.J. Blaker, Modulation of neuronal cell affinity on PEDOT-PSS nonwoven silk scaffolds for neural tissue engineering, ACS Biomater. Sci. Eng. 6 (12) (2020) 6906–6916, https://doi.org/10.1021/acsbiomaterials.0c01239.

[17] K. Roshanbinfar, L. Vogt, B. Greber, S. Diecke, A.R. Boccaccini, T. Scheibel, et al., Electroconductive biohybrid hydrogel for enhanced maturation and beating properties of engineered cardiac tissues, Adv. Funct. Mater. 28 (42) (2018), https://doi.org/10.1002/adfm.201803951.

[18] M.R. Abidian, E.D. Daneshvar, B.M. Egeland, D.R. Kipke, P.S. Cederna, M. G. Urbanchek, Hybrid conducting polymer-hydrogel conduits for axonal growth and neural tissue engineering, Adv. Healthcare Mater. 1 (6) (2012) 762–767, https://doi.org/10.1002/adhm.201200182.

[19] M.P. Prabhakaran, L. Ghasemi-Mobarakeh, G. Jin, S. Ramakrishna, Electrospun conducting polymer nanofibers and electrical stimulation of nerve stem cells, J. Biosci. Bioeng. 112 (5) (2011) 501–507, https://doi.org/10.1016/j.jbiosc.2011.07.010.

[20] J.M. Corey, D.Y. Lin, K.B. Mycek, Q. Chen, S. Samuel, E.L. Feldman, et al., Aligned electrospun nanofibers specify the direction of dorsal root ganglia neurite growth, J. Biomed. Mater. Res. 83 (3) (2007) 636–645, https://doi.org/10.1002/jbm.a.31285.

[21] S. Yoshii, M. Oka, M. Shima, A. Taniguchi, M. Akagi, 30 mm regeneration of rat sciatic nerve along collagen filaments, Brain Res. 949 (1–2) (2002) 202–208, https://doi.org/10.1016/s0006-8993(02)03149-9.

[22] M.I. Hassan, N.N. Masnawi, N. Sultana, Biomineralized conductive PEDOT: PSS-coated PLA/PHBV/HA nanofibrous membranes, Am. Soc. Artif. Intern. Organs J. 64 (3) (2018) 415–423, https://doi.org/10.1097/mat.0000000000000655.

[23] M. Pertea, G.M. Pertea, C.M. Antonescu, T.C. Chang, J.T. Mendell, S.L. Salzberg, StringTie enables improved reconstruction of a transcriptome from RNA-seq reads, Nat. Biotechnol. 33 (3) (2015) 290–295, https://doi.org/10.1038/nbt.3122.

[24] M.A. Barique, Y. Neo, M. Noyori, L. Aprila, M. Asai, H. Mimura, A large piezoelectric response in highly-aligned electrospun poly(vinylidene fluoride/trifluoroethylene) nanofiber webs for wearable energy harvesting, Nanotechnology 32 (1) (2021) 015401, https://doi.org/10.1088/1361-6528/abb5d3.

[25] L.G. Pozzobon, L.E. Sperling, C.E. Teixeira, T. Malysz, P. Pranke, Development of a conduit of PLGA-gelatin aligned nanofibers produced by electrospinning for peripheral nerve regeneration, Chem. Biol. Interact. 348 (2021) 109621, https://doi.org/10.1016/j.cbi.2021.109621.

[26] M. Ali, Y. Li, J.H. He, Double bubble electrospinning: patents and nanoscale interface, Recent Pat. Nanotechnol. (2023), https://doi.org/10.2174/0118722105259729231004040238.

[27] F. Ramacciotti, G. Sciutto, L. Cazals, D. Biagini, S. Reale, I. Degano, et al., Microporous electrospun nonwovens combined with green solvents for the selective peel-off of thin coatings from painting surfaces, J. Colloid Interface Sci. 663 (2024) 869–879, https://doi.org/10.1016/j.jcis.2024.03.006.

[28] M.F. Daud, K.C. Pawar, F. Claeyssens, A.J. Ryan, J.W. Haycock, An aligned 3D neuronal-glial co-culture model for peripheral nerve studies, Biomaterials 33 (25) (2012) 5901–5913, https://doi.org/10.1016/j.biomaterials.2012.05.008.
[29] M. Bognitzki, H.Q. Hou, M. Ishaque, T. Frese, M. Hellwig, C. Schwarte, et al., Polymer, metal, and hybrid nano- and mesotubes by coating degradable polymer template fibers (TUFT process), Adv. Mater. 12 (9) (2000) 637.
[30] M. Bognitzki, W. Czado, T. Frese, A. Schaper, M. Hellwig, M. Steinhart, et al., Nanostructured fibers via electrospinning, Adv. Mater. 13 (1) (2001) 70–+.
[31] S.R. Jang, J.I. Kim, C.H. Park, C.S. Kim, The controlled design of electrospun PCL/silk/quercetin fibrous tubular scaffold using a modified wound coil collector and L-shaped ground design for neural repair, Mater. Sci. Eng., C 111 (2020) 110776, https://doi.org/10.1016/j.msec.2020.110776.
[32] Q. Zhou, J. Xie, M. Bao, H. Yuan, Z. Ye, X. Lou, et al., Engineering aligned electrospun PLLA microfibers with nano-porous surface nanotopography for modulating the responses of vascular smooth muscle cells, J. Mater. Chem. B 3 (21) (2015) 4439–4450, https://doi.org/10.1039/c5tb00051c.
[33] L. Yao, N. O'Brien, A. Windebank, A. Pandit, Orienting neurite growth in electrospun fibrous neural conduits. Journal of biomedical materials research Part B, Applied biomaterials 90 (2) (2009) 483–491, https://doi.org/10.1002/jbm.b.31308.
[34] R. Zhu, Z. Sun, C. Li, S. Ramakrishna, K. Chiu, L. He, Electrical stimulation affects neural stem cell fate and function in vitro, Exp. Neurol. 319 (2019) 112963, https://doi.org/10.1016/j.expneurol.2019.112963.
[35] P.O. Osazuwa, C.Y. Lo, X. Feng, A. Nolin, C. Dhong, L.V. Kayser, Surface functionalization with (3-glycidyloxypropyl)trimethoxysilane (GOPS) as an alternative to blending for enhancing the aqueous stability and electronic performance of PEDOT:PSS thin films, ACS Appl. Mater. Interfaces (2023), https://doi.org/10.1021/acsami.3c09452.
[36] J. Plog, X. Wang, K.M. Lichade, Y. Pan, A.L. Yarin, Extremely-fast electrostatically-assisted direct ink writing of 2D, 2.5D and 3D functional traces of conducting polymer Poly(3,4-ethylenedioxythiophene) polystyrene sulfonate-polyethylene oxide (PEDOT:PSS-PEO), J. Colloid Interface Sci. 651 (2023) 1043–1053, https://doi.org/10.1016/j.jcis.2023.07.206.
[37] L. Ghasemi-Mobarakeh, M.P. Prabhakaran, M. Morshed, M.H. Nasr-Esfahani, H. Baharvand, S. Kiani, et al., Application of conductive polymers, scaffolds and electrical stimulation for nerve tissue engineering, Journal of tissue engineering and regenerative medicine 5 (4) (2011) e17–e35, https://doi.org/10.1002/term.383.
[38] A. Shahini, M. Yazdimamaghani, K.J. Walker, M.A. Eastman, H. Hatami-Marbini, B.J. Smith, et al., 3D conductive nanocomposite scaffold for bone tissue engineering, Int. J. Nanomed. 9 (2014) 167–181, https://doi.org/10.2147/ijn.s54668.
[39] N. Sultana, M. Wang, PHBV/PLLA-based composite scaffolds fabricated using an emulsion freezing/freeze-drying technique for bone tissue engineering: surface modification and in vitro biological evaluation, Biofabrication 4 (1) (2012) 015003, https://doi.org/10.1088/1758-5082/4/1/015003.
[40] M. Yazdimamaghani, M. Razavi, M. Mozafari, D. Vashaee, H. Kotturi, L. Tayebi, Biomineralization and biocompatibility studies of bone conductive scaffolds containing poly(3,4-ethylenedioxythiophene):poly(4-styrene sulfonate) (PEDOT:PSS), J. Mater. Sci. Mater. Med. 26 (12) (2015) 274, https://doi.org/10.1007/s10856-015-5599-8.
[41] A. Babaie, B. Bakhshandeh, A. Abedi, J. Mohammadnejad, I. Shabani, A. Ardeshirylajimi, et al., Synergistic effects of conductive PVA/PEDOT electrospun scaffolds and electrical stimulation for more effective neural tissue engineering, Eur. Polym. J. 140 (2020), https://doi.org/10.1016/j.eurpolymj.2020.110051.
[42] X. Niu, M. Rouabhia, N. Chiffot, M.W. King, Z. Zhang, An electrically conductive 3D scaffold based on a nonwoven web of poly(L-lactic acid) and conductive poly (3,4-ethylenedioxythiophene), J. Biomed. Mater. Res. 103 (8) (2015) 2635–2644, https://doi.org/10.1002/jbm.a.35408.
[43] H.C. Chang, T. Sun, N. Sultana, M.M. Lim, T.H. Khan, A.F. Ismail, Conductive PEDOT:PSS coated polylactide (PLA) and poly(3-hydroxybutyrate-co-3-hydroxyvalerate) (PHBV) electrospun membranes: fabrication and characterization, Mater. Sci. Eng., C 61 (2016) 396–410, https://doi.org/10.1016/j.msec.2015.12.074.
[44] T.A. Kung, N.B. Langhals, D.C. Martin, P.J. Johnson, P.S. Cederna, M. G. Urbanchek, Regenerative peripheral nerve interface viability and signal transduction with an implanted electrode, Plast. Reconstr. Surg. 133 (6) (2014) 1380–1394, https://doi.org/10.1097/prs.0000000000000168.
[45] T. Boretius, M. Schuettler, T. Stieglitz, On the stability of poly-ethylenedioxythiopene as coating material for active neural implants, Artif. Organs 35 (3) (2011) 245–248, https://doi.org/10.1111/j.1525-1594.2011.01210.x.
[46] Z.P. Zhou, C.L. Lai, L.F. Zhang, Y. Qian, H.Q. Hou, D.H. Reneker, et al., Development of carbon nanofibers from aligned electrospun polyacrylonitrile nanofiber bundles and characterization of their microstructural, electrical, and mechanical properties, Polymer 50 (13) (2009) 2999–3006, https://doi.org/10.1016/j.polymer.2009.04.058.
[47] H. Yan, H. Okuzaki, Effect of solvent on PEDOT/PSS nanometer-scaled thin films: XPS and STEM/AFM studies, Synth. Met. 159 (21–22) (2009) 2225–2228, https://doi.org/10.1016/j.synthmet.2009.07.032.
[48] Y.L. Wang, J. Hao, Z.Q. Huang, G.Q. Zheng, K. Dai, C.T. Liu, et al., Flexible electrically resistive-type strain sensors based on reduced graphene oxide-decorated electrospun polymer fibrous mats for human motion monitoring, Carbon 126 (2018) 360–371, https://doi.org/10.1016/j.carbon.2017.10.034.
[49] Y. Ding, W. Xu, W. Wang, H. Fong, Z. Zhu, Scalable and facile preparation of highly stretchable electrospun PEDOT:PSS@PU fibrous nonwovens toward wearable conductive textile applications, ACS Appl. Mater. Interfaces 9 (35) (2017) 30014–30023, https://doi.org/10.1021/acsami.7b06726.
[50] J.T. Reeder, Z. Xie, Q. Yang, M.H. Seo, Y. Yan, Y. Deng, et al., Soft, bioresorbable coolers for reversible conduction block of peripheral nerves, Science 377 (6601) (2022) 109–115, https://doi.org/10.1126/science.abl8532.
[51] M. MacEwan, L. Jeng, T. Kovács, E. Sallade, Clinical application of bioresorbable, synthetic, electrospun matrix in wound healing, Bioengineering (Basel, Switzerland) 10 (1) (2022), https://doi.org/10.3390/bioengineering10010009.
[52] A. Ai, E. Hasanzadeh, F. Safshekan, M.E. Astaneh, M. SalehiNamini, R. Naser, et al., Enhanced spinal cord regeneration by gelatin/alginate hydrogel scaffolds containing human endometrial stem cells and curcumin-loaded PLGA nanoparticles in rat, Life Sci. 330 (2023) 122035, https://doi.org/10.1016/j.lfs.2023.122035.
[53] Z. Li, P. Xu, L. Shang, B. Ma, H. Zhang, L. Fu, et al., 3D collagen porous scaffold carrying PLGA-PTX/SDF-1α recruits and promotes neural stem cell differentiation for spinal cord injury repair, J. Biomater. Sci. Polym. Ed. (2023) 1–24, https://doi.org/10.1080/09205063.2023.2247715.
[54] E. Yu, Z. Chen, Y. Huang, Y. Wu, Z. Wang, F. Wang, et al., A grooved conduit combined with decellularized tissues for peripheral nerve regeneration, J. Mater. Sci. Mater. Med. 34 (7) (2023) 35, https://doi.org/10.1007/s10856-023-06737-z.
[55] F. Liang, Y. Yang, Y. Chen, J. Xie, S. Liu, Z. Tan, et al., Ropivacaine microsphere-loaded electroconductive nerve dressings for long-acting analgesia and functional recovery following diabetic peripheral nerve injury, Materials today Bio 21 (2023) 100712, https://doi.org/10.1016/j.mtbio.2023.100712.
[56] A. Faroni, S.A. Mobasseri, P.J. Kingham, A.J. Reid, Peripheral nerve regeneration: experimental strategies and future perspectives, Adv. Drug Deliv. Rev. 82–83 (2015) 160–167, https://doi.org/10.1016/j.addr.2014.11.010.
[57] Y. Hou, X. Wang, Z. Zhang, J. Luo, Z. Cai, Y. Wang, et al., Repairing transected peripheral nerve using a biomimetic nerve guidance conduit containing intraluminal sponge fillers, Adv. Healthcare Mater. 8 (21) (2019) e1900913, https://doi.org/10.1002/adhm.201900913.
[58] W.A. Lackington, Z. Kočí, T. Alekseeva, A.J. Hibbitts, S.L. Kneafsey, G. Chen, et al., Controlling the dose-dependent, synergistic and temporal effects of NGF and GDNF by encapsulation in PLGA microparticles for use in nerve guidance conduits for the repair of large peripheral nerve defects, J. Contr. Release 304 (2019) 51–64, https://doi.org/10.1016/j.jconrel.2019.05.001.
[59] X. Jiao, B. Liu, X. Dong, S. Wang, X. Cai, H. Zhang, et al., Exploring PLGA-OH-CATH30 microspheres for oral therapy of Escherichia coli-induced enteritis, Biomolecules 14 (1) (2024), https://doi.org/10.3390/biom14010086.
[60] G. Mittal, D.K. Sahana, V. Bhardwaj, M.N. Ravi Kumar, Estradiol loaded PLGA nanoparticles for oral administration: effect of polymer molecular weight and copolymer composition on release behavior in vitro and in vivo, J. Contr. Release 119 (1) (2007) 77–85, https://doi.org/10.1016/j.jconrel.2007.01.016.
[61] Y. Yan, R. Yao, J. Zhao, K. Chen, L. Duan, T. Wang, et al., Implantable nerve guidance conduits: material combinations, multi-functional strategies and advanced engineering innovations, Bioact. Mater. 11 (2022) 57–76, https://doi.org/10.1016/j.bioactmat.2021.09.030.
[62] S. Park, Y.J. Kang, S. Majd, A review of patterned organic bioelectronic materials and their biomedical applications, Adv. Mater. 27 (46) (2015) 7583–7619, https://doi.org/10.1002/adma.201501809.
[63] G. Heywang, F. Jonas, POLY(ALKYLENEDIOXYTHIOPHENE)S - new, very stable conducting polymers, Adv. Mater. 4 (2) (1992) 116–118, https://doi.org/10.1002/adma.19920040213.
[64] M.R. Abidian, E.D. Daneshvar, B.M. Egeland, D.R. Kipke, P.S. Cederna, M. G. Urbanchek, Hybrid conducting polymer-hydrogel conduits for axonal growth and neural tissue engineering, Adv. Healthcare Mater. 1 (6) (2012) 762–767, https://doi.org/10.1002/adhm.201200182.
[65] L.H. Huang, J. Hu, L. Lang, X. Wang, P.B. Zhang, X.B. Jing, et al., Synthesis and characterization of electroactive and biodegradable ABA block copolymer of polylactide and aniline pentamer, Biomaterials 28 (10) (2007) 1741–1751, https://doi.org/10.1016/j.biomaterials.2006.12.007.
[66] M.B. Runge, M. Dadsetan, J. Baltrusaitis, A.M. Knight, T. Ruesink, E.A. Lazcano, et al., The development of electrically conductive polycaprolactone fumarate-polypyrrole composite materials for nerve regeneration, Biomaterials 31 (23) (2010) 5916–5926, https://doi.org/10.1016/j.biomaterials.2010.04.012.
[67] Y. Qian, H. Lin, Z.W. Yan, J.L. Shi, C.Y. Fan, Functional nanomaterials in peripheral nerve regeneration: scaffold design, chemical principles and microenvironmental remodeling, Mater. Today 51 (2021) 165–187, https://doi.org/10.1016/j.mattod.2021.09.014.
[68] P. Lu, G. Wang, T. Qian, X. Cai, P. Zhang, M. Li, et al., The balanced microenvironment regulated by the degradants of appropriate PLGA scaffolds and chitosan conduit promotes peripheral nerve regeneration, Materials today Bio 12 (2021) 100158, https://doi.org/10.1016/j.mtbio.2021.100158.
[69] X.F. Hu, Y.F. Feng, G. Xiang, W. Lei, L. Wang, Lactic acid of PLGA coating promotes angiogenesis on the interface between porous titanium and diabetic bone, J. Mater. Chem. B 6 (15) (2018) 2274–2288, https://doi.org/10.1039/c7tb03247a.
[70] P. Muangsanit, V. Roberton, E. Costa, J.B. Phillips, Engineered aligned endothelial cell structures in tethered collagen hydrogels promote peripheral nerve regeneration, Acta Biomater. 126 (2021) 224–237, https://doi.org/10.1016/j.actbio.2021.03.039.
[71] J.I. Rosales-Leal, M.A. Rodriguez-Valverde, G. Mazzaglia, P.J. Ramon-Torregrosa, L. Diaz-Rodriguez, O. Garcia-Martinez, et al., Effect of roughness, wettability and morphology of engineered titanium surfaces on osteoblast-like cell adhesion,

Colloids Surf., A 365 (1–3) (2010) 222–229, https://doi.org/10.1016/j.colsurfa.2009.12.017.
[72] M. Lampin, C. Warocquier, C. Legris, M. Degrange, M.F. Sigot-Luizard, Correlation between substratum roughness and wettability, cell adhesion, and cell migration, J. Biomed. Mater. Res. 36 (1) (1997) 99–108, https://doi.org/10.1002/(sici)1097-4636(199707)36:1<99::aid-jbm12>3.0.co;2-e.
[73] M. Anderson, N.B. Shelke, O.S. Manoukian, X. Yu, L.D. McCullough, S.G. Kumbar, Peripheral nerve regeneration strategies: electrically stimulating polymer based nerve growth conduits, Crit. Rev. Biomed. Eng. 43 (2–3) (2015) 131–159, https://doi.org/10.1615/CritRevBiomedEng.2015014015.
[74] S. Lu, W. Chen, J. Wang, Z. Guo, L. Xiao, L. Wei, et al., Polydopamine-Decorated PLCL conduit to induce synergetic effect of electrical stimulation and topological morphology for peripheral nerve regeneration, Small Methods 7 (2) (2023) e2200883, https://doi.org/10.1002/smtd.202200883.
[75] M. Zatkova, A. Reichova, Z. Bacova, V. Strbak, A. Kiss, J. Bakos, Neurite outgrowth stimulated by oxytocin is modulated by inhibition of the calcium voltage-gated channels, Cell. Mol. Neurobiol. 38 (1) (2018) 371–378, https://doi.org/10.1007/s10571-017-0503-3.
[76] S. Wang, S. Guan, W. Li, D. Ge, J. Xu, C. Sun, et al., 3D culture of neural stem cells within conductive PEDOT layer-assembled chitosan/gelatin scaffolds for neural tissue engineering, Mater. Sci. Eng., C 93 (2018) 890–901, https://doi.org/10.1016/j.msec.2018.08.054.
[77] C. Wang, L. Wu, R. Zhou, C. Song, P. Chen, S. Huang, et al., Integration of microbiota and metabolomics reveals the analgesic mechanisms of emodin against neuropathic pain, Int. Immunopharm. 125 (Pt A) (2023) 111170, https://doi.org/10.1016/j.intimp.2023.111170.
[78] J. Teissie, B.E. Knox, T.Y. Tsong, J. Wehrle, Synthesis of adenosine triphosphate in respiration-inhibited submitochondrial particles induced by microsecond electric pulses, Proc. Natl. Acad. Sci. U.S.A. 78 (12) (1981) 7473–7477, https://doi.org/10.1073/pnas.78.12.7473.
[79] H. Sauer, R. Stanelle, J. Hescheler, M. Wartenberg, The DC electrical-field-induced Ca(2+) response and growth stimulation of multicellular tumor spheroids are mediated by ATP release and purinergic receptor stimulation, J. Cell Sci. 115 (Pt 16) (2002) 3265–3273, https://doi.org/10.1242/jcs.115.16.3265.
[80] J.C. Seegers, M.L. Lottering, A.M. Joubert, F. Joubert, A. Koorts, C.A. Engelbrecht, et al., A pulsed DC electric field affects P2-purinergic receptor functions by altering the ATP levels in in vitro and in vivo systems, Med. Hypotheses 58 (2) (2002) 171–176, https://doi.org/10.1054/mehy.2001.1506.
[81] I. Titushkin, M. Cho, Regulation of cell cytoskeleton and membrane mechanics by electric field: role of linker proteins, Biophys. J. 96 (2) (2009) 717–728, https://doi.org/10.1016/j.bpj.2008.09.035.
[82] G. Thrivikraman, S.K. Boda, B. Basu, Unraveling the mechanistic effects of electric field stimulation towards directing stem cell fate and function: a tissue engineering perspective, Biomaterials 150 (2018) 60–86, https://doi.org/10.1016/j.biomaterials.2017.10.003.
[83] G. Bendale, M. Smith, L. Daniel, I. deBruler, M. Fernandes Gragnani, R. Clement, et al., In vivo efficacy of a novel, sutureless coaptation device for repairing peripheral nerve defects, Tissue Eng. 29 (17–18) (2023) 461–470, https://doi.org/10.1089/ten.TEA.2023.0004.
[84] W. Jing, Q. Ao, L. Wang, Z.R. Huang, Q. Cai, G.Q. Chen, et al., Constructing conductive conduit with conductive fibrous infilling for peripheral nerve regeneration, Chem. Eng. J. 345 (2018) 566–577, https://doi.org/10.1016/j.cej.2018.04.044.
[85] L.E. Kokai, Y.C. Lin, N.M. Oyster, K.G. Marra, Diffusion of soluble factors through degradable polymer nerve guides: controlling manufacturing parameters, Acta Biomater. 5 (7) (2009) 2540–2550, https://doi.org/10.1016/j.actbio.2009.03.009.
[86] Y. Qian, J. Song, X. Zhao, W. Chen, Y. Ouyang, W. Yuan, et al., 3D fabrication with integration molding of a graphene oxide/polycaprolactone nanoscaffold for neurite regeneration and angiogenesis, Adv. Sci. 5 (4) (2018) 1700499, https://doi.org/10.1002/advs.201700499.
[87] X. Yao, Y. Qian, C. Fan, Electroactive nanomaterials in the peripheral nerve regeneration, J. Mater. Chem. B 9 (35) (2021) 6958–6972, https://doi.org/10.1039/d1tb00686j.
[88] X. Zhang, L. Lu, Y. Zhong, L. Wang, Y. Ren, Comparison study of clinicopathological features of cellular schwannoma between retroperitoneum and other sites, Ann. Transl. Med. 10 (24) (2022) 1311, https://doi.org/10.21037/atm-22-4979.
[89] Y. Qian, X. Zhao, Q. Han, W. Chen, H. Li, W. Yuan, An integrated multi-layer 3D-fabrication of PDA/RGD coated graphene loaded PCL nanoscaffold for peripheral nerve restoration, Nat. Commun. 9 (1) (2018) 323, https://doi.org/10.1038/s41467-017-02598-7.
[90] S. Lee, X.Q. Shi, A. Fan, B. West, J. Zhang, Targeting macrophage and microglia activation with colony stimulating factor 1 receptor inhibitor is an effective strategy to treat injury-triggered neuropathic pain, Mol. Pain 14 (2018) 1744806918764979, https://doi.org/10.1177/1744806918764979.
[91] F.O. Martinez, S. Gordon, The M1 and M2 paradigm of macrophage activation: time for reassessment, F1000prime reports 6 (2014) 13, https://doi.org/10.12703/p6-13.
[92] K.A. Kigerl, J.C. Gensel, D.P. Ankeny, J.K. Alexander, D.J. Donnelly, P. G. Popovich, Identification of two distinct macrophage subsets with divergent effects causing either neurotoxicity or regeneration in the injured mouse spinal cord, J. Neurosci. : the official journal of the Society for Neuroscience 29 (43) (2009) 13435–13444, https://doi.org/10.1523/jneurosci.3257-09.2009.
[93] J.M. Wang, J.D. Griffin, A. Rambaldi, Z.G. Chen, A. Mantovani, Induction of monocyte migration by recombinant macrophage colony-stimulating factor, J. Immunol. 141 (2) (1988) 575–579 (Baltimore, Md : 1950).
[94] X.M. Dai, G.R. Ryan, A.J. Hapel, M.G. Dominguez, R.G. Russell, S. Kapp, et al., Targeted disruption of the mouse colony-stimulating factor 1 receptor gene results in osteopetrosis, mononuclear phagocyte deficiency, increased primitive progenitor cell frequencies, and reproductive defects, Blood 99 (1) (2002) 111–120, https://doi.org/10.1182/blood.v99.1.111.
[95] F. Porcheray, S. Viaud, A.C. Rimaniol, C. Léone, B. Samah, N. Dereuddre-Bosquet, et al., Macrophage activation switching: an asset for the resolution of inflammation, Clin. Exp. Immunol. 142 (3) (2005) 481–489, https://doi.org/10.1111/j.1365-2249.2005.02934.x.
[96] A.J. Fleetwood, T. Lawrence, J.A. Hamilton, A.D. Cook, Granulocyte-macrophage colony-stimulating factor (CSF) and macrophage CSF-dependent macrophage phenotypes display differences in cytokine profiles and transcription factor activities: implications for CSF blockade in inflammation, J. Immunol. 178 (8) (2007) 5245–5252, https://doi.org/10.4049/jimmunol.178.8.5245.
[97] X. Lu, R. Yu, Z. Li, M. Yang, J. Dai, M. Liu, JC-010a, a novel selective SHP2 allosteric inhibitor, overcomes RTK/non-RTK-mediated drug resistance in multiple oncogene-addicted cancers, Cancer Lett. 582 (2024) 216517, https://doi.org/10.1016/j.canlet.2023.216517.
[98] H. Xuan, B. Li, F. Xiong, S. Wu, Z. Zhang, Y. Yang, et al., Tailoring nano-porous surface of aligned electrospun poly (L-Lactic acid) fibers for nerve tissue engineering, Int. J. Mol. Sci. 22 (7) (2021), https://doi.org/10.3390/ijms22073536.
[99] B. Sun, T. Wu, J. Wang, D. Li, J. Wang, Q. Gao, et al., Polypyrrole-coated poly(l-lactic acid-co-ε-caprolactone)/silk fibroin nanofibrous membranes promoting neural cell proliferation and differentiation with electrical stimulation, J. Mater. Chem. B 4 (41) (2016) 6670–6679, https://doi.org/10.1039/c6tb01710j.
[100] A.N. Koppes, A.L. Nordberg, G.M. Paolillo, N.M. Goodsell, H.A. Darwish, L. Zhang, et al., Electrical stimulation of schwann cells promotes sustained increases in neurite outgrowth, Tissue Eng. 20 (3–4) (2014) 494–506, https://doi.org/10.1089/ten.TEA.2013.0012.
[101] H. Zhang, D. Lan, B. Wu, X. Chen, X. Li, Z. Li, et al., Electrospun piezoelectric scaffold with external mechanical stimulation for promoting regeneration of peripheral nerve injury, Biomacromolecules 24 (7) (2023) 3268–3282, https://doi.org/10.1021/acs.biomac.3c00311.